

Bioorganic & Medicinal Chemistry

**Thermodynamics and Kinetic Studies in the Binding  
Interaction of Cyclic Naphthalene Diimide Derivatives  
with Double Stranded DNAs**

**Md. Monirul Islam,<sup>a</sup> Satoshi Fujii,<sup>b</sup> Shinobu Sato,<sup>a</sup> Tatsuo Okauchi,<sup>a</sup>  
and Shigeori Takenaka<sup>a\*</sup>**

<sup>a</sup>Department of Applied Chemistry, Kyushu Institute of Technology, Kitakyushu,  
Fukuoka, 804-8550 Japan,

<sup>b</sup>Department of Bioscience and Bioinformatics, Kyushu Institute of Technology, Iizuka,  
Fukuoka, 820-8502 Japan.

**Corresponding author**

Shigeori Takenaka, Ph.D.

Department of Applied Chemistry,

Kyushu Institute of Technology

Kitakyushu, Fukuoka

804-8550, Japan

Tel&Fax: +81-93-884-3322

shige@che.kyutech.ac.jp

© 2015. This manuscript version is made available under the CC-BY-NC-ND 4.0 license  
<http://creativecommons.org/licenses/by-nc-nd/4.0/>

## **ABSTRACT**

Previously, we reported our investigations of the interaction between a cyclic naphthalene diimide derivative (cNDI **1**) and double stranded DNA (dsDNA) (Czerwinska, I. et al. *Bioorg. Med. Chem.* 22 (2014) 2593–260. Here, we report the synthesis of the novel cNDI **2**, which has shorter linker chains than cNDI **1**. We performed comparative investigations of the interactions of both cNDI **1** and cNDI **2** with different types of dsDNA, including analysis of their thermodynamics and kinetics. Interactions between the cNDIs and calf thymus DNA (CT-DNA), poly[d(A-T)]<sub>2</sub>, or poly[d(G-C)]<sub>2</sub> were explored by physicochemical and biochemical methods, including UV-Vis spectroscopy, circular dichroism (CD) spectroscopy, stopped-flow kinetics, and a topoisomerase I assay. Upon addition of cNDIs to CT-DNA, the existence of an induced CD signal at approximately the wavelength of the naphthalene diimide chromophore and unwinding of the DNA duplex, as detected by the topoisomerase I assay, revealed that cNDIs bound to the DNA duplex. As indicated by the steric constraint in the formation of the complex, bis-threading intercalation was the more favorable binding mode. UV-Vis spectroscopic titration of the cNDIs with DNA duplexes showed affinities on the order of  $10^5$ – $10^6$  M<sup>-1</sup>, with a stoichiometry of one cNDI molecule per four DNA base pairs. Thermodynamic parameters ( $\Delta G$ ,  $\Delta H$ , and  $\Delta S$ ) based on the van't Hoff equation indicated that exothermic and entropy-dependent hydrophobic interactions played a major role in the reaction. Stopped-flow association and dissociation analysis showed that cNDI interactions with poly[d(G-C)]<sub>2</sub> were more stable and had a slower dissociation rate than their interactions with poly[d(A-T)]<sub>2</sub> and CT-DNA. Measurement of ionic strength indicated that electrostatic attraction is also an important component of the interaction between cNDIs and CT-DNA. Because of its longer linker chain, cNDI **1** showed higher binding selectivity, a more entropically favorable interaction, and much slower dissociation from dsDNA than cNDI **2**.

## **Keywords**

Cyclic naphthalene diimide derivatives, Double-stranded DNA, Bis-intercalative binding, Entropy-dependence binding, Hydrophobic interaction

## 1. Introduction

Because small molecules that bind to DNA affect numerous functions of living organisms, such molecules have potential as therapeutic agents that function by controlling gene expression. Thus, the study of interactions between DNA and small molecules is vital in chemical and biological drug discovery research.<sup>1,2</sup> It is important to study the thermodynamics and kinetics of the interactions between small molecules and DNA in order to understand the binding modes of these molecules and develop new, effective, DNA-targeted drugs.<sup>1</sup> Accordingly, many small molecule drugs that interact with DNA have been investigated.<sup>3</sup> A classical intercalating drug slides between adjacent base pairs of a DNA duplex and forms a stable complex, resulting in mutations, such as frameshift.<sup>5</sup> A threading intercalating drug is a new type of intercalator; in its interaction with DNA, two substituents of the molecule are located on the major and minor grooves of the DNA duplex, preventing dissociation.<sup>2</sup> Nogalamycin is a typical threading intercalator, and its antitumor activity is correlated with its DNA dissociation rate constant.<sup>2</sup> This exemplifies the relationship between physical data and biological activity. It also shows the importance of physical studies of the interactions between small molecules and DNA duplexes.

Expanding on threading intercalating drugs, bis-intercalators have also been utilized to stabilize the DNA complex.<sup>1-4</sup> Chaires et al. developed the bis-intercalating drug daunomycin.<sup>2</sup> Like nogalamycin, this molecule's slower dissociation rate correlates with its biological activity. Recently, the same concept has been explored for bis-intercalating or cyclic intercalating derivatives of naphthalene diimide.<sup>5-10</sup> The interaction of a cyclic naphthalene diimide with DNA shows a unique catenated structure that dramatically stabilizes the complex. A new type of cyclic naphthalene diimide, cNDI **1**, which is connected with its substituent through the benzene ring, can stabilize both a DNA duplex and a DNA tetraplex.<sup>11,12</sup> In recent years, the synthesis of bis-intercalators has drawn considerable attention because of the drugs' potential superiority over mono-intercalators. Higher DNA-binding constants, slower dissociation rates, and substantial sequence selectivity can be expected from the incorporation of two or more intercalating units into a polyfunctional ligand.<sup>6,7</sup>

Researchers have already reported that naphthalene diimide derivatives act as DNA-targeting anticancer agents, and such derivatives have shown potent activity against cancer cell lines and telomerase.<sup>13,14</sup> Depending on the substituents, naphthalene diimide derivatives have shown selectivity toward AT- or GC-rich regions of DNA.<sup>4,6</sup> We previously published our synthesis and evaluation of the binding of G-quadruplex

and dsDNA with cNDI **1** and other cNDIs.<sup>11,12</sup> In the present study, the interaction of cNDI **1** and the newly designed cNDI **2** with dsDNA was analyzed by UV-Vis spectroscopy, CD spectroscopy, a topoisomerase I assay, and stopped-flow kinetics to characterize differences in binding mode and binding selectivity.

## **Fig. 1**

## **2. Experimental procedure**

### *2.1. Materials*

CT-DNA, poly[d(A-T)]<sub>2</sub>, and poly d[(G-C)]<sub>2</sub> synthetic polymers were obtained from Sigma-Aldrich (St. Louis, MO). The following extinction coefficients ( $\epsilon$ ) were used for quantification of the nucleic acid solutions: 12824 M<sup>-1</sup> cm<sup>-1</sup> for CT-DNA, 13200 M<sup>-1</sup> cm<sup>-1</sup> for poly[d(A-T)]<sub>2</sub>, and 16800 M<sup>-1</sup> cm<sup>-1</sup> for poly[d(G-C)]<sub>2</sub>. Details of the synthesis procedure for cNDIs **1** and **2** are described in the supplementary data, and a non-cyclic NDI **3** was synthesized as previously described.<sup>15</sup> We obtained 2.0 M KCl and 5.0 M NaCl aqueous solutions from Life Technologies (Carlsbad, CA), 1.0 M Tris-HCl (pH 7.4) buffer from Sigma-Aldrich (St. Louis, MO), and 2-Morpholinoethanesulfonic acid (MES) from Dojindo (Japan)

### *2.2. UV-Vis titration experiments*

Absorption spectra were measured using the Hitachi U-3310 spectrophotometer with a 1-cm path-length quartz cell and were recorded in the 200–600 nm range at 25°C. UV-Vis absorption titrations were carried out by the stepwise addition of 3 mM/base pair of CT-DNA, poly[d(A-T)]<sub>2</sub>, or poly[d(G-C)]<sub>2</sub> to a UV cell containing 6.7  $\mu$ M solutions of cNDIs **1–3**. The measurements were performed in 10 mM MES buffer (pH 6.25) containing 100 mM NaCl and 1 mM EDTA. Binding data, which were obtained by spectrophotometric titration of increasing concentrations of each drug to a fixed concentration of DNA, were analyzed by Scatchard plot analysis of  $r/C$  versus  $r$ , according to the excluded-site model of the McGhee-von Hippel equation.<sup>16</sup> (Eq. 1). The binding data were analyzed with KaleidaGraph software, using the Levenberg-Marquardt algorithm to determine parameters  $K_b$  and  $n$ .

### *2.3. Thermodynamics analysis*

The effect of temperature on ligand binding affinity was investigated to derive the thermodynamic functions of ligand-DNA complex formation. Absorption spectra were measured at 20, 22.5, 25, and 27.5°C. Titrations were performed under conditions similar to those used in the UV-Vis titration experiments. Enthalpy change ( $\Delta H$ ) and entropy change ( $\Delta S$ ) were measured by the van't Hoff equation plotted against  $\ln K$  versus  $1/T$  (Eq. 2). The free energy change ( $\Delta G$ ) was estimated by the Gibbs free energy equation (Eq. 3).

#### 2.4. Salt effect analysis

Salt-dependent Scatchard analysis was conducted at five different concentrations of sodium salt: 50, 75, 100, 125, and 150 mM. Titrations were performed under similar conditions as those used for the UV-Vis titration experiments. The strength of electrostatic interactions of the ligand was determined by plotting the negative logarithm of the sodium salt concentration ( $\log [\text{Na}^+]$ ) against the binding constant ( $\log K$ ) (Eq. 4).

#### 2.5. Stopped flow kinetics experiments

Stopped-flow kinetic experiments were performed with the SF-61 DX2 double mixing stopped-flow system (Hi-Tech Scientific Inc., Salisbury, UK) equipped with a Lauda RF206 temperature controller. Samples were prepared in a buffer solution (10 mM MES, 1 mM EDTA, and 0.1 M NaCl; pH 6.25). Absorbance was measured at the maximum absorption of the cNDI derivatives. Association rate constants of the ligand-dsDNA interactions were obtained by fitting the exponential traces of absorbance observed after mixing the ligand solution with DNA at a 10-fold excess of the ligand concentration. The dual-exponential equation was used for nonlinear fitting:  $A_1 \exp(k_1 t) + A_2 \exp(k_2 t)$ , where  $A$  and  $k$  refer to the fractional amplitudes and rate constants, respectively. The intrinsic second-order association rate constant ( $k_a$ ) and the dissociation rate constants ( $k_d$ ) were obtained from the slope and intercept of a plot of the apparent association rate constant ( $k_{app} = A_1 k_1 + A_2 k_2$ ) against the DNA concentration, according to the equation  $k_{app} = k_a [\text{DNA}] + k_d$ . The dissociation rate constant ( $k_d$ ) of the ligand from DNA was independently determined by sodium dodecyl sulfate (SDS)-driven dissociation measurements, as described previously.<sup>14, 15</sup> Equal volumes of 1% SDS solution and the DNA-ligand complex were mixed instantaneously using a piston pump. Changes in absorbance over time were recorded. When the

DNA-ligand complex was mixed with SDS solution, the free ligand underwent incorporation into the SDS micelles. As this reaction is diffusion-controlled, all absorption changes represent a  $k_d$ -dependent process; therefore nonlinear fitting of the kinetic trace provides the  $k_d$  value.

## 2.6. Topoisomerase I assay measurements

A topoisomerase I assay was carried out according to the method previously reported.<sup>11,12</sup> Briefly, 0.25  $\mu\text{g}$  of pUC19 was incubated with 5 U of topoisomerase I in 0.1% bovine serum albumin (BSA) and  $1\times$  reaction buffer—composed of 35 mM Tris-HCl (pH 8.0), 72 mM potassium chloride, 5 mM magnesium chloride, 5 mM dithiothreitol (DTT), and 5 mM spermidine—at 37°C for 5 min. Various concentrations of cNDI derivatives **1–3** were then added, and the mixture was incubated at 37°C for 1 h. The reaction was terminated by the addition of 2  $\mu\text{L}$  of 10% sodium dodecylsulfate (SDS) and 0.5  $\mu\text{L}$  of 20 mg/ml proteinase K, and the solution was then incubated at 37°C for 15 min. Topoisomerase I was then extracted with phenol containing chloroform and isoamyl alcohol, and then with chloroform containing isoamyl alcohol. After ethanol precipitation and dissolution, topoisomerase I was analyzed by gel electrophoresis on 1% agarose in  $1\times$  TAE at 18 V for 3.5 h. The gel was stained with Gelstar (Takara Bio, Shiga, Japan) in  $1\times$  TAE for 30 min.

## 2.7. Circular dichroism (CD) measurements

Various concentrations (5–50  $\mu\text{M}$ ) of cNDI derivatives **1–3** were added to 100  $\mu\text{M}$ /base pair CT-DNA in 10 mM MES buffer (pH 6.25) containing 100 mM NaCl and 1 mM EDTA at 25°C. CD spectra were taken at a scan rate of 50 nm/min on a Jasco J-820 spectropolarimeter (Tokyo, Japan). Scan parameters were as follows: response = 2 s, data interval = 0.1 nm, sensitivity = 100 mdeg, band width = 2 nm, and scan number = 4.

## 2.8. Computer modeling

Molecular models of the cNDI-DNA complexes were constructed by MOE 2011.10 (<http://www.chemcomp.com/>). cNDI **1** or **2** was placed on the binding site of the DNA duplex, and energy minimization of the complex was carried out. Molecular dynamics calculation of the mineralized complex was further carried out until cNDI **1** or **2** was

stabilized in the binding site. Finally, energy minimization of the complex was obtained, as shown in Fig. 6. These calculations were performed using the force field of MMFF94x.

### 3. Result and discussions

#### 3.1. Binding studies of cNDIs- dsDNAs: UV-Vis titrations

Spectroscopic titration of cNDIs with dsDNAs was carried out. The interaction showed maximum absorption at 383 nm and a large hypochromic effect with a small redshift, indicative of binding between the cNDIs and the dsDNAs (Fig. S7). An example of the spectrophotometric titration of cNDI **1** with CT-DNA is illustrated in Fig. 1A. The observed hypochromic effect indicated strong intercalative binding of cNDIs between dsDNAs. Optical data of the cNDIs are shown in Table S1. An isosbestic point observed at 395 nm supports the prediction of a two-state system involving bound and free cNDIs. Absorbance at a specific wavelength indicated the participation of both free and bound cNDIs when titrated with a fixed concentration of DNA. Scatchard plots were prepared using absorption changes at the specific wavelength 383 nm upon the addition of various concentrations of dsDNA. We used the data in a range of approximately 30%–80% bound region of cNDI and dsDNA. The Scatchard plot in Fig. 2B illustrates binding between the cNDIs and dsDNAs. It was analyzed using the McGhee-von Hippel equation<sup>16</sup> (Eq. 1) for non-cooperative ligand binding.

$$\frac{v}{C} = K(1 - nv) \left( \frac{1-nv}{1-(n-1)v} \right)^{n-1} \quad (1)$$

$v$  is the stoichiometry (the number of ligand molecules bound per moles of base pair),  $C$  is the free ligand concentration,  $K$  is the observed binding constant ( $K_b$ ), and  $n$  is the number of base pairs excluded by the binding of a single ligand molecule. The solid line in B indicates a good fit of the experimental values to those predicted by the McGhee-von Hippel equation. Scatchard analysis using the spectra change of cNDIs upon the addition of dsDNAs showed binding constants ranging from  $1.0\text{--}53.4 \times 10^5 \text{ M}^{-1}$ , and the observed binding order was  $\text{poly}[\text{d}(\text{G-C})]_2 > \text{CT-DNA} > \text{poly}[\text{d}(\text{A-T})]_2$ . The expected value of  $n$  was four, as cNDIs interact with dsDNAs by bis-intercalation of four base pairs, whereas the threading intercalator non-cyclic NDI **3** followed the nearest-neighbor exclusion principle,<sup>16</sup> in which it bound with dsDNAs by intercalation of two base pairs. We expected a violation of the nearest-neighbor exclusion principle

by the cNDIs because they are large, cyclic macromolecules; a single cNDI molecule may cover more than two DNA base pairs and bind with dsDNA in bis-intercalative mode. Previous reports<sup>11, 12</sup> on the binding of NDI derivatives to DNAs have shown similar trends of spectral change and support the binding constant for non-cyclic NDI **3** observed here. Previously, we reported that the interaction between cNDI **1** and duplex oligonucleotides revealed a higher binding constant ( $3.7 \times 10^6 \text{ M}^{-1}$ ) and melting temperature than did the interaction between non-cyclic NDI **3** and duplex oligonucleotides.<sup>11</sup> We further studied cNDIs **1–3** with different types of dsDNA that carried AT- or GC-rich sequences to determine the sequence specificity of binding. cNDI **1** and cNDI **2** showed similar trends of binding behavior with the different types of dsDNA. cNDIs **1** and **2** showed comparatively higher binding affinity to dsDNAs than NDI **3** (Table 1) because of the binding flexibility of NDI **3**. The moiety of NDI **3** may intercalate between dsDNA base pairs, and does not depend on major and minor groove binding. On other hand, cNDI intercalated with the major and minor grooves of dsDNA makes a rigid catenane complex.<sup>8</sup> Our observations revealed that long-chain cNDI **1** has higher binding affinity to dsDNAs than short-chain cNDI **2**. According to computer modeling, short-chain cNDI **2** may have a steric strain effect in its binding with dsDNA. In addition, Sato et al. previously reported that the introduction of a methyl or alkyl group results in a higher binding constant because of the substituent effect.<sup>17</sup> We have already reported that other types of short-chain cNDI derivatives may have a greater affinity for G-quadruplex DNA than for DNA duplex because of a stacking interaction between the short-chain cNDI derivatives and G-quadruplex DNA.<sup>12</sup> cNDI **1** displayed the highest affinity for poly[d(G-C)]<sub>2</sub>, with a binding constant of  $5.34 \times 10^6 \text{ M}^{-1}$ , which is approximately 9 times higher than the binding constant of its interactions with CT-DNA and Poly[d(A-T)]<sub>2</sub> (Table 2). There is a strong tendency for cNDIs to bind with GC base pairs because of the rigidity, depth, and width of the GC groove. Nucleophilic guanine may also have a strong affinity for protonated cNDI molecules.<sup>18</sup> We assumed that cNDIs may strongly intercalate 5'-GpC-3' sequences by insertion of the naphthalene diimide moiety and benzene ring into the 5'-GC/CG-3' step, creating a catenane structure with dsDNA.<sup>19</sup> Preferential interactions of NDI ligands with GC polymers have been observed previously, confirming that the binding affinity of NDIs varies with DNA sequence.<sup>20</sup> Additionally, the double-stranded DNA structure is known to be highly dynamic in solution, with base pairs opening and reforming rapidly at room temperature. cNDIs may be able to exploit this millisecond “breathing” behavior of dsDNA by sliding between the temporarily disrupted DNA base pairs to form a pseudo-catenane or bis-intercalation complex structure.<sup>21</sup> Under natural conditions,

DNA dynamic breathing is also referred to as “partial base flipping.”<sup>22, 23</sup> Recently, Nakatani et al. reported that a single-molecule ligand can, in fact, induce nucleotide base flipping.<sup>24</sup> Overall, the present study is consistent with previous investigations of the interaction between cNDIs and dsDNAs, which have included bis-intercalators such as bisacridine and bisdaunamycin.<sup>25, 26</sup> The binding of cNDIs to dsDNAs (Fig. 6) is structurally similar to cNDI-dsDNA structures previously described by other groups.<sup>8</sup>

## Fig. 2

## Table 1

### 3.2. Thermodynamic analysis

The interaction between a drug and biomolecule may involve hydrophobic forces, electrostatic interactions, van der Waals interactions, hydrogen bonds, and other forces. According to data on enthalpy changes ( $\Delta H$ ) and entropy changes ( $\Delta S$ ), the following model of interaction between a drug and a biomolecule can be concluded: (1)  $\Delta H > 0$  and  $\Delta S > 0$ , hydrophobic forces; (2)  $\Delta H < 0$  and  $\Delta S < 0$ , van der Waals interactions and hydrogen bonds; (3)  $\Delta H < 0$  and  $\Delta S > 0$ , electrostatic interactions.<sup>27</sup> When there is little change in temperature,  $\Delta H$  can be considered constant, and its value, along with that of  $\Delta S$ , can be determined from the van't Hoff (Eq. 2) and Gibbs free energy (Eq. 3) equations.

$$\ln K_b = -\frac{\Delta H}{RT} + \frac{\Delta S}{R} \quad (2)$$

$$\Delta G = \Delta H - T\Delta S \quad (3)$$

$K_b$  is the binding constant at the corresponding temperature and R is the gas constant. The values of  $\Delta H$  and  $\Delta S$  were obtained from the slope and intercept of the linear plot (Eq. 2) of  $\ln K$  against  $1/T$  (Fig. S8). The value of  $\Delta G$  was estimated from Eq. (3). Its negative value means that the binding process is spontaneous (Table 2). The values of  $\Delta H$  and  $\Delta S$  for the binding between cNDI derivatives **13** and CT-DNA are listed in Table 2. The positive enthalpy and positive entropy values of the interaction between cNDI **1** or **2** and CT-DNA indicate that hydrophobic forces played a major role in the reaction. These results are consistent with previously reported results for binding between CT-DNA and NDI derivatives.<sup>28</sup> When cNDI **1** or **2** interacts with CT-DNA, the driving force of the interaction clearly changes from enthalpy to entropy. The

change in entropy is governed by the release of counterions and water from both DNA and the ligand, and also by changes in the local DNA structure upon ligand binding. These features simultaneously contribute unfavorable  $\Delta H$  and favorable  $\Delta S$  to the binding free energy and have been observed by other researchers.<sup>29,30</sup> Spolar et al. have also reported that the entropy change depends on the rigidity of the DNA-protein complexes.<sup>30</sup> Moreover, the intercalating chromophore of cNDI consists of two aromatic ring systems that intercalate into the DNA duplex in a parallel arrangement that follows the lock and key model, making its stability entropically driven.<sup>3,30</sup> Binding between the bis-intercalator echinomycin and DNA has been shown to be entropically and hydrophobically driven, which is in agreement with our observations of binding between the newly designed cNDIs and CT-DNA.<sup>3,31</sup> According to thermodynamic data, we can state that long-chain cNDI **1** was more favorable for entropy-dependent binding than short-chain cNDI **2**.

## **Table 2**

### *3.3. Salt effect analysis*

The entropic nature of the reaction can be related to the significant role of hydrophobic interactions in binding process. Thus the electrostatic effect is almost entirely enthalpic.<sup>27,32</sup> In our study, Electrostatic interaction is less important for cNDIs binding to DNA because of favorable entropy. The binding constant of cNDIs to DNA entirely depends on salt concentration even though cNDIs is neutral charged. Reports in the past have shown that a very high concentration of NaCl would hinder small molecules from binding with DNA.<sup>33</sup> Our results show that the binding parameters decreased with a gradual increase in NaCl concentration (Table S3). According to counterion condensation theory (Eq. 4) is a measure of the number of sodium ions released from DNA per bound ligand. Due to the lengthening of the DNA helix and unwinding DNA upon intercalation, increasing the phosphate gaps along the helix axis.<sup>17, 29, 34</sup> Consequently, releasing condensed counterions because of the charge density of the duplex decreases and providing an entropically favorable contribution to the binding free energy. Releasing counterions explains the dramatic salt dependencies of DNA-cNDIs complexes. High salt destabilizes DNA- cNDIs complexes. There is a large entropic gain from counterion release, if the salt concentration in solution is low and the cNDIs binds tightly to the DNA. The entropic gain from counterion release is small, if the salt concentration in solution is high and the cNDIs binds weakly. We

observed that an increased salt concentration hindered the binding of cNDI **1** more significantly than that of cNDI **2**. At pH 6.25, the net charge would have been different because cNDI **1** possesses four nitrogen atoms in the linker whereas cNDI **2** possesses only two. Moreover, at low ionic strength, a cNDI molecule binds to DNA with a large number of ion pairs, consequently increasing the free energy association through the release of a large fraction of counterions; this effect would be dramatically reduced at high ionic strength.<sup>35</sup> According to the polyelectrolyte theory,<sup>36</sup> we plotted  $\log K$  against  $-\log [\text{Na}^+]$  in Fig. S10, and the slope was given by Eq. 4.

$$\frac{\delta \log K_{obs}}{\delta \log [\text{Na}^+]} = -m\Psi \quad (4)$$

Where  $m$  is the charge on the ligand and  $\Psi$  is the proportion of counterions associated with each DNA phosphate group. Normally  $\Psi$  is 0.88 for monocationic classical intercalator and is its twice for dicationic one with double-stranded *B*-type DNA.<sup>2, 32</sup> However, it is known that  $\Psi$  is 0.6 – 0.8 even for dicationic threading intercalators.<sup>15</sup> The data in Table 3 show slopes of 0.72, 0.74 and 0.83 for cNDI derivatives **1**, **2**, and **3**, respectively. This result suggested that these dicationic cNDI derivatives behave as threading intercalator and form catenane complex with double stranded DNA.

### Table 3

#### 3.4. Stopped flow kinetic analysis

As suggested in our previous report<sup>11</sup> cNDI **1** showed a much slower dissociation constant in its interaction with GC than cNDI **3**. In the present report, we have discussed in detail the association and dissociation kinetics of cNDI derivatives **1–3**.

*Association:* Typical examples of the association kinetic traces of the interactions of CT-DNA, Poly[d(A-T)]<sub>2</sub>, and Poly[d(G-C)]<sub>2</sub> with cNDI derivatives **1–3** are shown in Figs. 3A and 4A. All data were analyzed by two-exponential fitting, and the results are summarized in Table 4. The highest absorption by the DNA duplex-ligand complex occurred at 383 nm (Fig. 4A). Absorption decreased dramatically and underwent a slight bathochromic shift. This phenomenon has previously been observed for interactions between other naphthalene diimide derivatives and dsDNAs.<sup>15</sup> Association rate constants for cNDI derivatives **1–3** increased in the following order: Poly[d(A-T)]<sub>2</sub>, CT-DNA, Poly[d(G-C)]<sub>2</sub>. The association process of the interaction of cNDI **1** with poly[d(A-T)]<sub>2</sub> was about two and five times higher than that of non-cyclic NDI **3** and

cNDI **2**, respectively. The association kinetics of cNDI derivatives **1-3** with poly[d(G-C)]<sub>2</sub> were almost two times slower than with poly[d(A-T)]<sub>2</sub>, implying that transient breathing of the double helix influences the rate of association. Previous reports on naphthalene diimides derivatives as tri-intercalators have shown similar association constant trends.<sup>5</sup> Indeed, a study of the kinetics of the threading intercalator anthracene also noted a similar association trend that may be related to a rate-determining DNA breathing step.<sup>37</sup> In addition, the association rate constant may depend on the cyclic character and rigidity of the ligand molecule. Thus, the side chains of the ligand molecule can have large effects on DNA interaction kinetics. Complex formation can be slowed by the disruption of a higher number of adjacent base pairs when two intercalation sites open in the double helix.

*Dissociation:* A typical example of the SDS-driven dissociation kinetic traces of interactions between CT-DNA, Poly[d(A-T)]<sub>2</sub>, or Poly[d(G-C)]<sub>2</sub> and cNDI derivatives **1-3** is shown in Figs. 3B and 4B. All data were analyzed by two-exponential fitting, and the results are summarized in Table 4. The highest absorption by the DNA duplex-ligand complex occurred at 383 nm (Fig. 4A). Absorption decreased dramatically and underwent a slight bathochromic shift. This phenomenon has previously been observed for interactions between other naphthalene diimide derivatives and dsDNAs.<sup>15</sup> Dissociation rate constants for cNDI derivatives **1-3** increased in the following order: Poly[d(G-C)]<sub>2</sub>, CT-DNA, Poly[d(A-T)]<sub>2</sub>. It is worth mentioning the very slow dissociation of cNDI **1** from the GC-rich complex, which was 100 times slower than that of non-cyclic NDI **3** and 330 times slower than that of cNDI **2**. This is due to the strong binding constant of the interaction between cNDIs and GC-rich dsDNA (Table 1) because of the rigidity of the complex, as previously discussed. Many heterocyclic or highly polarizable intercalators exhibit a binding preference for GC base pairs with a larger asymmetric charge distribution. Although the cNDIs that we have synthesized are symmetric, they still have significant partial atomic charges on the heterocyclic rings, and the molecule in Fig. 1 for example, exhibits significant GC binding specificity. These results are similar to previously reported dissociation rate constants for interactions between naphthalene diimide derivatives and CT-DNA, which were lower for GC-rich sequences than for AT-rich sequences.<sup>5</sup> A study of the kinetics of the threading intercalator anthracene also noted a similar dissociation trend.<sup>37</sup> These effects are related to the high binding affinity of cNDIs **1** and **2** for poly[d(G-C)]<sub>2</sub>, resulting from hydrophobic interactions, favorable van der Waals stacking interactions of the large naphthalene diimide ring system, and partial atomic

charges on the heterocyclic rings that can provide favorable coulombic interactions, particularly with GC base pairs. Long-chain cNDI **1** showed slower dissociation from dsDNA than short-chain cNDI **2**. Researchers have already found that longer chain bis-intercalators and poly-intercalators dissociate slowly from DNA duplexes.<sup>5</sup>

#### **Table 4**

#### **Fig. 3**

#### **Fig. 4**

### *3.5. Topoisomerase I assay*

Topoisomerase-based gel assays have been widely used to evaluate compounds for their ability to intercalate DNA.<sup>38</sup> The ability of NDI derivatives to cause re-supercoiling of plasmid DNA has been frequently reported.<sup>11,12</sup> The topoisomerase I assay exploits the ability of the topoisomerase I enzyme to relax supercoiled DNA (e.g., pUC19-plasmid DNA). In the presence of an intercalator, the enzyme will convert the relaxed DNA into a supercoiled state by unwinding and lightening of the DNA structure. Previously, we reported that cNDI derivatives **1** and **3** are DNA intercalators.<sup>11, 12</sup> In the present study, plasmid DNA was treated with increasing concentrations of cNDI **2** in the presence of topoisomerase I. Complete re-supercoiling of the plasmid DNA upon interaction with cNDI **2** was readily observed, indicating its identity as a DNA intercalator (Fig. S14). Remarkably, cNDI **1** elicited re-supercoiling more effectively than cNDI **2**. cNDI **1** re-supercoiled DNA completely at a concentration of ca. 2  $\mu$ M, whereas the concentration of cNDI **2** required to show a similar effect exceeded ca. 10  $\mu$ M. These results are in agreement with the higher binding affinity of cNDI **1** for DNA duplexes.

### *3.6. Circular dichroism experiments*

Intrinsic and induced CD spectroscopy was used to further elucidate the conformational aspects of the interaction between cNDIs and CT-DNA. The characteristic CD spectrum of right-handed B-form DNA in the 200–300 nm region can provide information indicating specific structural changes in DNA upon interaction with ligands. Previously, we reported that cNDI derivatives **1** and **3** induce a negative CD

band (in the 340–440 nm region) upon interaction with CT-DNA, Poly [d(A-T)]<sub>2</sub>, or Poly [d(G-C)]<sub>2</sub>, indicating an intercalative binding mode.<sup>11</sup> cNDI derivatives **1** and **3** also showed a dramatic change in the CD spectrum in the region of 220–320 nm, indicating that the ligands affect duplex stability and conformation.<sup>11</sup> In the present study, we used CD spectroscopy to investigate the interaction between cNDI **2** and CT-DNA. As depicted in the CD spectrum (Fig. 5A), we observed a negative peak around 245 nm for free CT-DNA, due to helicity, and a positive peak around 276 nm, due to base stacking. After the addition of cNDI **2**, the positive and negative CD bands increased rapidly without any shift in the band position. We also observed a small negative band around the 320–400 nm region (Fig. 5B). These bands indicated that binding of CT-DNA had reached the saturation point. In light of previous reports,<sup>39</sup> the negative CD band associated with cNDI **2**-CT-DNA complexes may indicate that cNDIs **1** and **2** intercalate with the long axis of the chromophore oriented parallel or perpendicular to the long axis of the DNA base pair.<sup>10</sup> cNDI **1** induced higher CD spectra than cNDI **2** and non-cyclic NDI **3**, in agreement with its stronger binding to DNA duplexes DNA than that of cNDI **2**.

**Fig. 5**

**Fig. 6**

### *3.7. Computer modeling*

Computer modeling of the structures of the cNDI **1**- and cNDI **2**-dsDNA complexes is shown in Fig. 6. Previously, we reported the binding mode of cNDI **1** with dsDNA. Here we propose a similar binding mode, with bis-threading intercalation or formation of a pseudo-catenate complex between cNDI **1** or **2** and dsDNA, which is consistent with a model previously published by Iverson et al.<sup>8</sup> Computer modeling suggests that the cNDI **2**-dsDNA complex has a steric strain effect, due to the shorter linker chain.

## **4. Conclusions**

We have developed a new type of bis-intercalator, cNDI **2**, which was synthesized by the cyclization of naphthalene diimide (NDI). We previously reported our investigation of the interaction between cNDI **1** and dsDNA.<sup>11</sup> Here we compare the interaction

between cNDI **1** and dsDNA with that of cNDI **2** and dsDNA. The result of interaction studies of cNDI derivatives **1–3** with dsDNAs follows the order **1** > **2** > **3**, which suggests that the long-chain cNDI **1** has higher ds DNA binding selectivity and binds dsDNA with more favorable thermodynamics and kinetics than cNDI **2**. UV-Vis analysis showed high binding affinity of cNDI **1** to dsDNA in the range of  $6 \times 10^5$ – $5.3 \times 10^6$  M<sup>-1</sup> (approximately 10 times higher than that of cNDI **2**), with bis-intercalation of four base pairs per ligand molecule. Thermodynamic studies of cNDIs **1** and **2** indicated that entropy-dependent hydrophobic interactions play a major role in their interaction with dsDNA. cNDI **1** showed more entropically favorable interactions with dsDNA than cNDI **2**. Kinetics studies of cNDIs **1** and **2** indicated that cNDI **1** dissociate from GC base pairs more slowly than cNDI **2** because of its unique, pseudo-catenane, bis-intercalative binding with stairs of dsDNA. Induced CD spectra and a topoisomerase I unwinding assay further supported the more favorable bis-intercalation binding of cNDI **1** over that of cNDI **2**.

### **Acknowledgements**

This work was supported in part by Grants-in-Aid for Scientific Research from Ministry of Education, Culture, Sports, Science, and Technology (MEXT), Japan.

### **Supplementary data**

Supplementary data (synthesis of cNDI **1** & **2**, <sup>1</sup>H-NMR spectra, HPLC spectra, HRMS-EI & HRMS-FAB spectra, UV-Vis absorption spectra, Stopped-flow kinetics traces, Fig. of Topoisomerase I assay of cNDI **2** and others) associated with this article can be found, in the online version, at (*Web address*).

### **References and notes**

1. J.B. Chaires, Drug-DNA interactions, *Curr Opin Struct Biol.* 8 (1998) 314-20.
2. G.M. Blackburn, M.J. Gait, D. Loakes, D.M. Williams, *Nucleic Acids in Chemistry and Biology*, 3rd Ed., RSC Publication, Thomas Graham House, Science Park, Milton Road, Cambridge CB4 0WF, UK, 2006.
3. J.B. Chaires, A thermodynamic signature for drug–DNA binding mode, *Arch. Biochem. Biophys.* 453 (2006) 26–31.
4. V.M. Guelev, M.S. Cubberley, M.M. Murr, R.S. Lokey, B.L. Iverson, *Design*,

- synthesis, and characterization of polyintercalating ligands, in: Chaires, J. B., and Waring, M. J., (Eds.), *Methods in Enzymol.* Academic Press, New York. 2001, pp 556-570.
5. R.S. Lokey, Y. Kwok, V. Guelev, C.J. Pursell, L.H. Hurley, B.L. Iverson, A New Class of Polyintercalating Molecules, *J. Am. Chem. Soc.* 119 (1997) 7202-7210.
  6. G.G. Holman, M. Zewail-Foote, A.R. Smith, K.A. Johnson, B.L. Iverson, A sequence-specific threading tetra-intercalator with an extremely slow dissociation rate constant, *Nat Chem.* 3 (2011) 875-881.
  7. A.R. Smith, B.L. Iverson, Threading Polyintercalators with Extremely Slow Dissociation Rates and Extended DNA Binding Sites, *Am. Chem. Soc.* 135 (2013) 12783–12789.
  8. Y. Chu, D.W. Hoffman, B.L. Iverson, A Pseudocatenane Structure Formed between DNA and A Cyclic Bisintercalator, *J. Am. Chem. Soc.* 131 (2009) 3499–3508.
  9. Y. Chu, S. Sorey, D.W. Hoffman, B.L. Iverson, Structural Characterization of a Rigidified Threading Bisintercalator, *J. Am. Chem. Soc.* 129 (2007) 1304-1311
  10. J. Lee, V. Guelev, S. Sorey, D.W. Hoffman, B.L. Iverson, NMR Structural Analysis of a Modular Threading Tetraintercalator Bound to DNA, *J. Am. Chem. Soc.* 126 (2004) 14036-14042
  11. I. Czerwinska, S. Sato, B. Juskowiak, S. Takenaka, Interactions of cyclic and non-cyclic naphthalene diimide derivatives with different nucleic acids, *Bioorg. Med. Chem.* 22 (2014) 2593–2601.
  12. Y. Esaki, M.M. Islam, S. Fujii, S. Sato, S. Takenaka, Design of tetraplex specific ligands: cyclic naphthalene diimide, *Chem. Commun.* 50 (2014) 5967-5969.
  13. A. Milelli, V. Tumiatti, M. Micco, M. Rosini, G. Zuccari, L. Raffaghello, G. Bianchi, V. Pistoia, J.F. Diaz, B. Pera, C. Trigili, I. Barasoain, C. Musetti, M. Toniolo, C. Sissi, S. Alcaro, F. Moraca, M. Zini, C. Stefanelli, A. Minarini, Structure activity relationships of novel substituted naphthalene diimides as anticancer agents, *Eur. J. Med. Chem.* 57 (2012) 417-428.
  14. S.M. Hampel, A. Sidibe, M. Gunaratnam, J.F. Riou, S. Neidle, Tetrasubstituted naphthalene diimide ligands with selectivity for telomeric G-quadruplexes and cancer cells, *Bioorg. Med. Chem. Lett.* 20 (2010) 6459–6463.
  15. F.A. Tanious, S.F. Yen, W.D. Wilson, Kinetic and Equilibrium Analysis of a Threading Intercalation Mode: DNA Sequence and Ion Effects, *Biochemistry* 30

- (1991) 1813–1819.
16. J.D. McGhee, P.H. von Hippel, Theoretical aspects of DNA-protein interactions: Co-operative and non-co-operative binding of large ligands to a one-dimensional homogeneous lattice, *J. Mol. Biol.* 86 (974) 469–489.
  17. Y. Sato, S. Nishizawa, K. Yoshimoto, T. Seino, T. Ichihashi, K. Morita, N. Teramae, Influence of substituent modifications on the binding of 2-amino-1,8-naphthyridines to cytosine opposite an AP site in DNA duplexes: thermodynamic characterization, *Nucleic Acids Res.* 37 (2009) 1411–1422.
  18. W.C. Tse, D.L. Boger, Sequence-Selective DNA Recognition: Natural Products and Nature's Lessons, *Chem. Biol.* 11 (2004) 1607–1617.
  19. Z.R. Liu, K.H. Hecker, R.L. Rill, Selective DNA Binding of (N-alkylamine) Substituted Naphthalene Imides and Diimides to G+C-rich DNA, *J. Biomol. Struct. Dyn.* 14 (1996) 331-339.
  20. R.E. McKnight, Insights into the Relative DNA Binding Affinity and Preferred Binding Mode of Homologous Compounds Using Isothermal Titration Calorimetry (ITC) in: A.A. Elkordy (Eds.), *Applications of Calorimetry in a Wide Context- Differential Scanning Calorimetry, Isothermal Titration Calorimetry and Microcalorimetry*, InTech publication, Rijeka, Croatia, 2013, pp. 129-152.
  21. P.H. vonHippel, N.P. Johnson, A.H. Marcus, 50 years of DNA 'Breathing': Reflections on Old and New Approaches, *Biopolymers* 99 (2013) 923–954.
  22. N. Huang; K.B. Nilesh; D.M. Alexander, Protein-facilitated base flipping in DNA by cytosine-5-methyltransferase, *PNAS* 100 (1) 68–73.
  23. N.K. Banavali, Partial Base Flipping Is Sufficient for Strand Slippage near DNA Duplex Termini, *J. Am. Chem. Soc.* 135 (2013) 8274–8282.
  24. K. Nakatani, S. Hagihara, Y. Goto, A. Kobori, M. Hagihara, G. Hayashi, M. Kyo, M. Nomura, M. Mishima, C. Kojima, Small-molecule ligand induces nucleotide flipping in (CAG)<sub>n</sub> trinucleotide repeats *Nat. Chem. Biol.* 1 (2005) 39-43.
  25. J.B. Chaires, F. Leng, T. Przewloka, I. Fokt, Y.H. Ling, R.P. Soler, W. Priebe, Structure-Based Design of a New Bisintercalating Anthracycline Antibiotic, *J. Med. Chem.* 40 (1997) 261-266.
  26. G.G. Hu, X. Shui, F. Leng, W. Priebe, J.B. Chaires, L.D. Williams, Structure of a DNA-Bisdaunomycin Complex, *Biochemistry* 36 (1997) 5940-5946.

27. N. Shahabadi, A. Fatahi, Multispectroscopic DNA-binding studies of a tris-chelate nickel(II) complex containing 4,7-diphenyl 1,10-phenanthroline ligands, *J. Mol. Struct.* 970 (2010) 90–95.
28. I. Haq, Thermodynamics of drug–DNA interactions, *Arch. Biochem. Biophys.* 403 (2002) 1-15.
29. H. Becker, B. Norden, DNA Binding Properties of 2,7-Diazapyrene and Its *N*-Methylated Cations Studied by Linear and Circular Dichroism Spectroscopy and Calorimetry, *J. Am. Chem. Soc.* 119 (1997) 5798-5803.
30. R.S. Spolar, M.T. Record Jr, Coupling of Local Folding to Site-Specific Binding of Proteins to DNA, *Science* 263 (1994) 777-784.
31. F. Leng, J.B. Chaires, M.J. Waring, Energetics of echinomycin binding to DNA, *Nucleic Acids Res.* 31 (2003) 7202-6197.
32. I. Haq, J.E. Ladbury, B.Z. Chowdhry, T.C. Jenkins, and J.B. Chaires, Specific Binding of Hoechst 33258 to the d(CGCAAATTTGCG)<sub>2</sub> Duplex: Calorimetric and Spectroscopic Studies, *J. Mol. Biol.* 271 (1997) 244-257.
33. W.D. Wilson, F.A. Tanious, Kinetic analysis of drug-nucleic acid binding modes: absolute rates and effects of salt concentration in: Neidle, S. and Waring, M. (Eds), *Molecular Aspects of Anticancer Drug–DNA Interactions*. CRC Press, MacMillan, London, 1994 Vol. 2, pp. 243–269.
34. M.T. Record, C.F. Anderson, T.M. Lohman, Thermodynamic analysis of ion effects on binding and conformational equilibrium of proteins and nucleic-acids roles of ion association or release, screening and ion effects on water activity, *Q.Rev. Biophys.* 11 (1978) 103–178.
35. R.L. Jones, A.C. Lanier, R.A. Keel, W.D. Wilson, The effect of ionic strength on DNA-ligand unwinding angles for acridine and quinoline derivatives, *Nucleic Acids Res.*, 8 (1980) 1613–1624.
36. W.D. Wilson, C.R. Krishnamoorthy, Y.H. Wang, J.C. Smith, Mechanism of Intercalation: Ion Effects on the Equilibrium and Kinetic Constants for the Interaction of Propidium and Ethidium with DNA, *Biopolymers* 24 (1985) 1941-1961.
37. F.A. Tanious, T.C. Jenkins, S. Neidle, W.D. Wilson, Substituent Position Dictates the Intercalative DNA-Binding Mode for Anthracene-9,10-dione Antitumor Drugs, *Biochemistry* 31 (1992) 11632-11640.
38. P. Peixoto, C. Bailly, M.H. David-Cordonnier, Topoisomerase I-mediated DNA

relaxation as a tool to study intercalation of small molecule into supercoiled DNA, *Methods Mol. Biol.* 613 (2010) 235-256.

39. M. Monnot, O. Mauffret, E. Lescot, S. Fermandjian, Probing intercalation and conformational effects of the anticancer drug 2-methyl-9-hydroxyellipticinium acetate in DNA fragments with circular dichroism, *Eur. J. Biochem.* 204 (1992) 1035-1039.

Table 1 Binding parameters of cNDI derivatives **1-3** with CT-DNA, Ploy [d(A-T)]<sub>2</sub> and Poly [d(G-C)]<sub>2</sub>

DNAs	<b>1</b>		<b>2</b>		<b>3</b>	
	$10^{-6}K_b/M^{-1}$	n	$10^{-6}K_b/M^{-1}$	n	$10^{-6}K_b/M^{-1}$	n
CT-DNA	0.7± 0.01	4.5	0.12± 0.005	4.9	0.34±0.006	3.4
Poly [d(A-T)] <sub>2</sub>	0.6± 0.055	3	0.10± 0.004	5	0.28±0.001	3
Poly [d(G-C)] <sub>2</sub>	5.34± 0.6	4	0.5 ± 0.013	3.5	0.84±0.026	2.2

Condition: 10 mM MES (pH6.25), 1 mM EDTA, and 0.1 M NaCl.

Table 2 Thermodynamic parameters of binding of cNDI derivatives **1-3** to calf thymus DNA.

Parameters	<b>1</b>	<b>2</b>	<b>3</b>
$\Delta H/kcal\ mol^{-1}$	7.8±1	9.2±0.84	-6.7±0.67
$\Delta S/cal\ mol^{-1}$	52.8±3.3	54.4±2.8	3±2
$\Delta G/kcal\ mol^{-1}$ (25 °C)	-7.95	-7.0	-7.59

Condition: 10 mM MES (pH6.25), 1 mM EDTA, and 0.1 M NaCl.

Table 3 Salt effects of cNDI derivatives **1-3** in the binding affinity.

cNDI derivatives	<b>1</b>	<b>2</b>	<b>3</b>
$\delta(\log K_{abs})/ \delta(\log[Na^+])$	0.72	0.74	0.83

Condition: 10 mM MES (pH6.25), 1 mM EDTA, and 0.05-0. 125 M NaCl.

Table 4 Kinetic parameters for binding of cNDI derivatives **1-3** to calf thymus DNA (CT-DNA), poly [d(A-T)]<sub>2</sub>, and poly [(G-C)]<sub>2</sub>.

DNAs	<b>1</b>		<b>2</b>		<b>3</b>	
	$10^{-5}k_a/M^{-1}s^{-1}$	$k_d/s^{-1}$	$10^{-5}k_a/M^{-1}s^{-1}$	$k_d/s^{-1}$	$10^{-5}k_a/M^{-1}s^{-1}$	$k_d/s^{-1}$
Calf thymus DNA	0.57±0.03	0.1	1.2±0.11	1.1	1.24±0.14	1.1
poly [d(A-T)] <sub>2</sub>	1.2±0.11	0.15	0.32±0.08	4.2	2.6±0.35	2.6
poly [d(G-C)] <sub>2</sub>	0.34±0.045	0.003	0.26±0.058	1.0	0.84±0.1	0.3

Condition: 10 mM MES (pH6.25), 1 mM EDTA, 0.1 M NaCl.

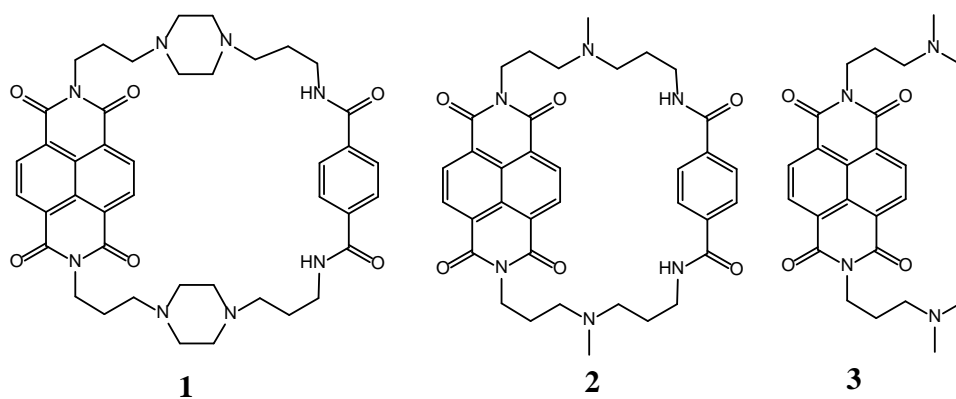


Fig. 1. Chemical structure of cNDI **1**, **2** and NDI **3**

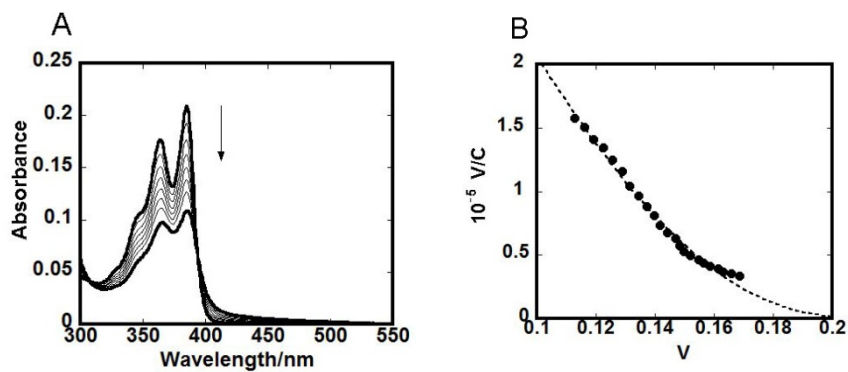


Fig. 2. Spectral shifts of 6.7  $\mu\text{M}$  of cNDI **1** on titration with 0, 5, 10, 15, 20, 25, 30, 40 and 50  $\mu\text{M}$  Calf thymus DNA (A) (from top to bottom). Scatchard plots for the binding of cNDI **1** to Calf thymus DNA (B). Experiments were performed at 25°C in 10 mM MES buffer pH 6.25 containing 100 mM NaCl and 1 mM EDTA.

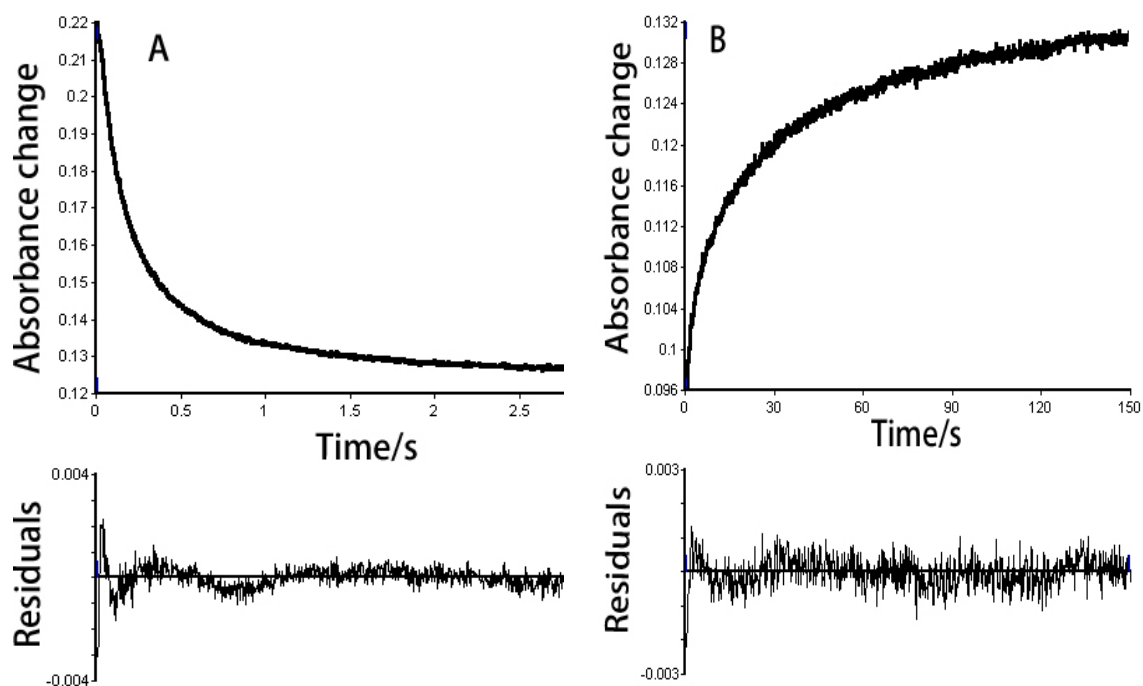


Fig. 3. Stopped-flow kinetic traces for the association (A) and the SDS-driven dissociation (B) for a complex of cNDI **1** with calf thymus DNA. The smooth line represents the two-exponential fit to the data. A residual plot for the fit showed under the experimental plot. The experiments were conducted at 25 °C in 10 mM MES buffer and 1mM EDTA with 0.1 M NaCl and the concentration of cNDI **1** to DNA base pair ratio of 1:10.

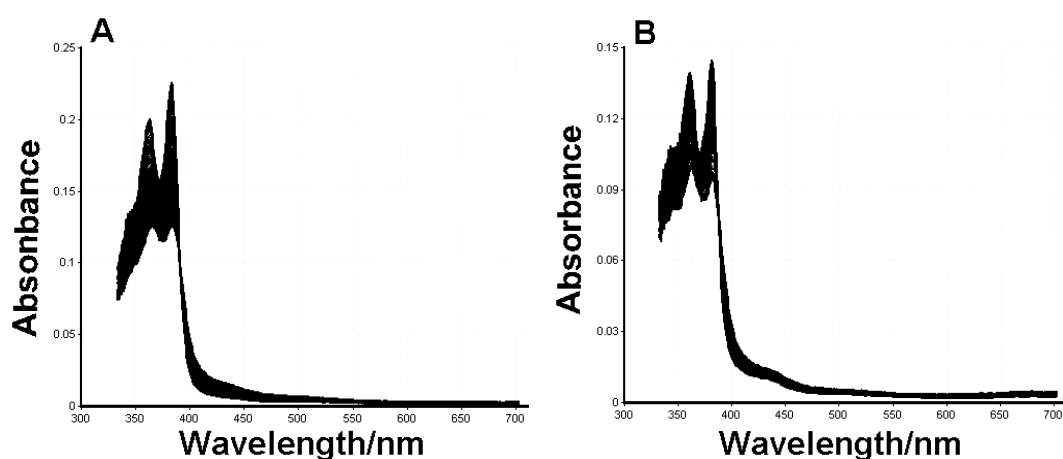


Fig. 4. Stopped-flow kinetic traces of absorption spectra at 383 nm for (A) association (B) SDS-driven dissociation for a complex of cNDI **1** with calf thymus DNA. The experimental condition was under the same condition described in Fig. 3.

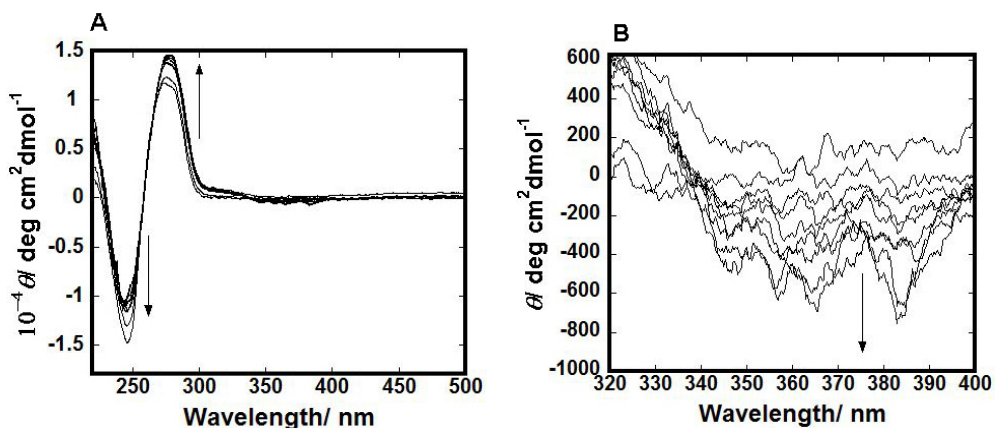


Fig. 5. (A) CD spectra of 100  $\mu$ M DNA samples titrated with cNDI **2** (0, 5, 10, 15, 20, 25, 30, 40 and  $\mu$ M from bottom to top) at 25°C in 10 mM MES buffer and 1 mM EDTA (pH 6.25) containing 100 mM NaCl. (B) Induced CD spectra at wavelength region 320-400 nm.

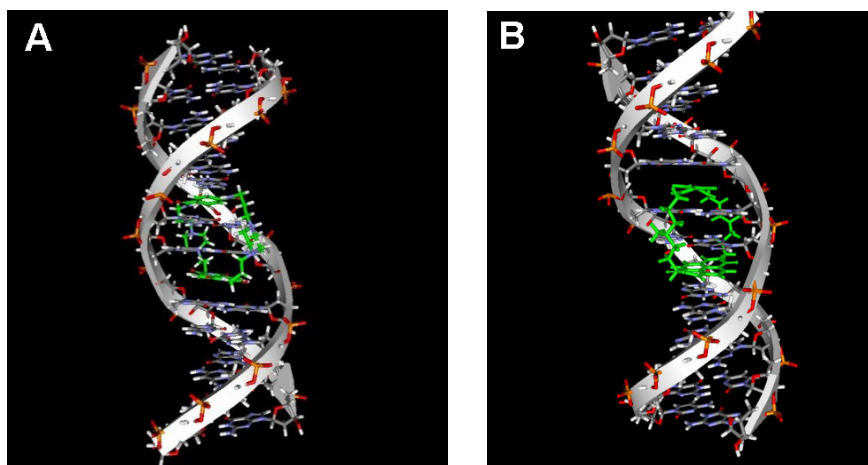


Fig. 6. Computer modeling of the complex of cNDI **1** (A) and cNDI **2** (A) with dsDNAs.

## Supplementary data

### Thermodynamics, Kinetic Studies in the Binding Interaction of Cyclic Naphthalene Diimide Derivatives with Double Stranded DNAs

Md. Monirul Islam,<sup>a</sup> Satoshi Fujii,<sup>b</sup> Shinobu Sato,<sup>a</sup> Tatsuo Okauchi,<sup>a</sup> Shigeori Takenaka<sup>a\*</sup>

<sup>a</sup>Department of Applied Chemistry, Kyushu Institute of Technology, Tobata, Kitakyushu, 804-8550 Japan, <sup>b</sup>Department of Bioscience and Bioinformatics, Kyushu Institute of Technology, Iizuka, Fukuoka, 820-8502 Japan.

List of Supporting Information data		Pages
	Synthesis of cNDI <b>1</b>	02
Fig. S1.	Reversed phase HPLC of cNDI <b>1</b>	03
Fig. S2.	<sup>1</sup> H-NMR chart of cNDI <b>1</b> in CDCl <sub>3</sub> using TMS as internal standard.	04
Fig. S3.	High-resolution mass spectra (HRMS-FAB) of cNDI <b>1</b> .	05
	Synthesis of cNDI <b>2</b>	06
Fig. S4.	Reversed phase HPLC of cNDI <b>2</b> .	07
Fig. S5.	<sup>1</sup> H-NMR chart of cNDI <b>2</b> in CDCl <sub>3</sub> using TMS as internal standard.	08
Fig. S6.	High-resolution mass spectra (HRMS-EI <sup>+</sup> ) of cNDI <b>2</b> .	09
Fig. S7.	UV-Vis absorption spectra of 6.7 μM of cNDI derivatives <b>1-3</b> with dsDNA	10
Table S1	Summary of the optical properties of free and DNA bound cNDIs derivatives	11
Fig. S8.	Plots of ln <i>K</i> , the observed equilibrium constants, vs 1/ <i>T</i> under the binding of cNDI derivatives <b>1-3</b> to calf thymus DNA	12
Table S2	Binding constants of cNDI derivatives <b>1-3</b> interacting with calf thymus DNA at different temperature.	13
Fig. S9.	UV-Vis absorption spectra of 6.7 μM of cNDI <b>1</b> with dsDNA at different temperature	14
Fig. S10.	Plots of log <i>K</i> , versus -log [Na <sup>+</sup> ] under the binding of cNDI derivatives <b>1-3</b> to calf thymus DNA.	15
Table S3	Binding constants of cNDI derivatives <b>1-3</b> interacting with calf thymus DNA at different salt concentration	16
Fig. S11.	Plot of the apparent rate constants ( <i>K</i> <sub>app</sub> ) against DNA concentrations	17
Fig. S12.	Stopped-flow kinetics traces for association of cNDI derivatives <b>1-3</b>	18
Fig. S13.	Stopped-flow kinetics traces for SDS driven dissociation of cNDI derivatives <b>1-3</b>	19

Fig. S14.	Topoisomerase I assay of cNDI 2	20
-----------	---------------------------------	----

### Synthesis of cyclic naphthalene diimide **1** and **2**

As precursors of **1** and **2**, N,N'-bis[[4-(3-aminopropyl)piperazinyl]propyl]-naphthalene-1,4,5,8-tetracarboxylic acid diimide (**4**) and N,N'-bis[3-(3-aminopropyl)methylaminopropyl] naphthalene-1,4,5,8-tetracarboxylic acid diimide (**5**) were synthesized according to the procedure reported previously [1]. **3** was synthesized according to the procedure reported previously [2].

[1] S, Sato, S. Takenaka, J. Organomet. Chem. 693 (2009) 1177-1185.

[2] F.A. Tanious, S.F. Yen, W.D. Wilson, Biochemistry 30 (1991) 1813-1819.

### Synthesis of cNDI **1**

A solution of **4** 1.0 g (1.5 mmol), terephthalic acid 0.25 g (1.5 mmol), triethylamine 12 mL, 1-hydroxybenzotriazole (HOBt) 0.60 g (4.5 mmol), 1H-Benzotriazol-1-yloxy-tri(pyrrolidino)phosphonium hexafluorophosphate (PyBOP) 2.3 g (4.5 mmol) in CHCl<sub>3</sub> 500 mL was stirred at room temperature and the progress of this reaction was monitored by TLC on silica gel with mixture of CHCl<sub>3</sub>: diethylamine = 10: 1.0 as developing agent. After 48 h stirring where the TLC spot of NDI (R<sub>f</sub>=0) was disappeared, the reaction mixture was evaporated under reduced pressure and the residue was dissolved with 20 mL CHCl<sub>3</sub>. After filtration and subsequently evaporation under reduced pressure, the residue was chromatographed on a silica gel column (Merck 60) using the eluent of CHCl<sub>3</sub> : diethylamine = 10: 1.0. The fraction of R<sub>f</sub>= 0.33 was collected and the solvent was removed under reduced pressure. The obtained residue was recrystallized from ethyl acetate, and cNDI **1** was obtained as brown crystal with 0.11 g (yield, 10%). MALDI-TOFMS (positive mode, α-CHCA) m/z =763.73 (theory for C<sub>42</sub>H<sub>50</sub>N<sub>8</sub>O<sub>6</sub>+H<sup>+</sup>= 763.90). <sup>1</sup>H NMR (250 MHz, CDCl<sub>3</sub>, TMS) δ1.54 (8H, m), 1.98 (4H, t, J = 6.0 Hz), 2.15 (6H, m), 2.29 (12H, m), 2.48 (4H, t, J=6.5 Hz), 3.44 (4H, m), 4.35 (4H, m, J = 6.0 Hz), 7.80 (4H, s), and 8.77(4H, s) ppm; HRMS Calcd. for C<sub>42</sub>H<sub>50</sub>N<sub>8</sub>O<sub>6</sub>+H<sup>+</sup>: M, 763.55. Found: m/z 763.55. 1 mM cNDI **1** aqueous solution was prepared as estimation from the molar absorptivity of 28800 cm<sup>-1</sup>M<sup>-1</sup> at 384 nm.

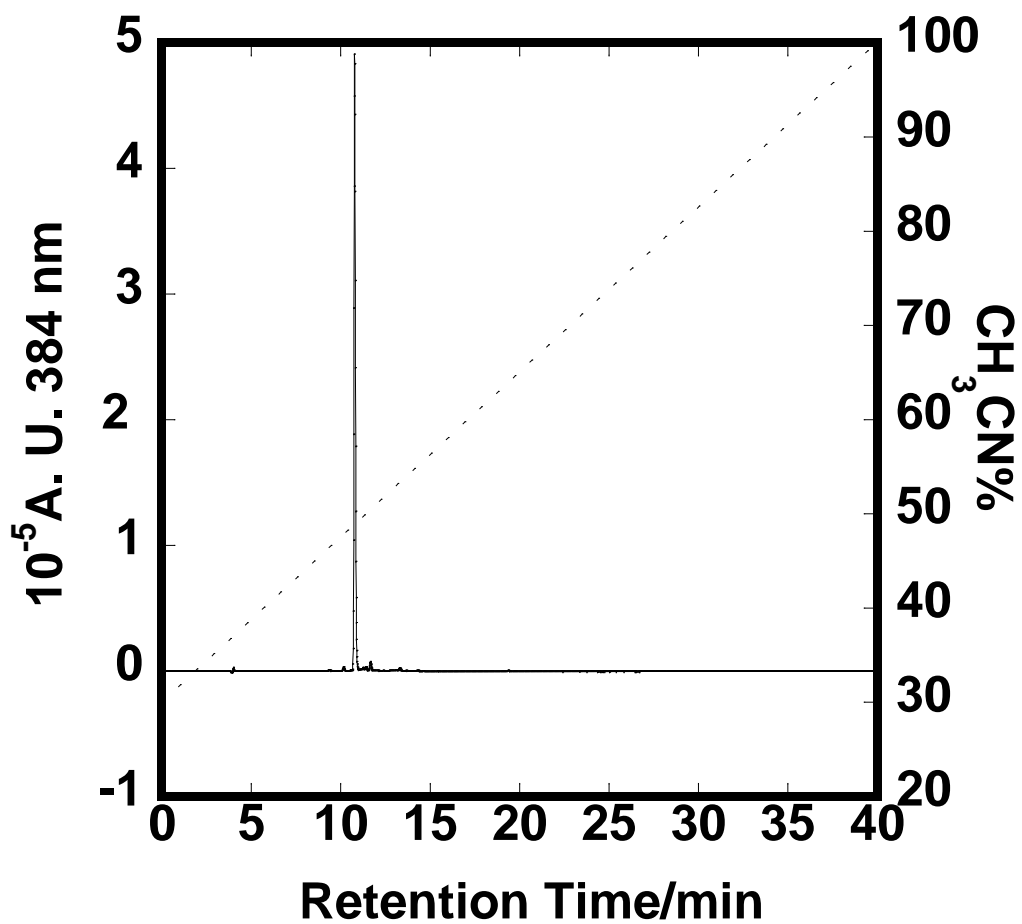


**Figure S1.** Reversed phase HPLC of cNDI 1. The concentration of acetonitrile was changed linearly to 100% from 28% in water containing 0.1% trifluoroacetic acid over 40 min at 40 °C

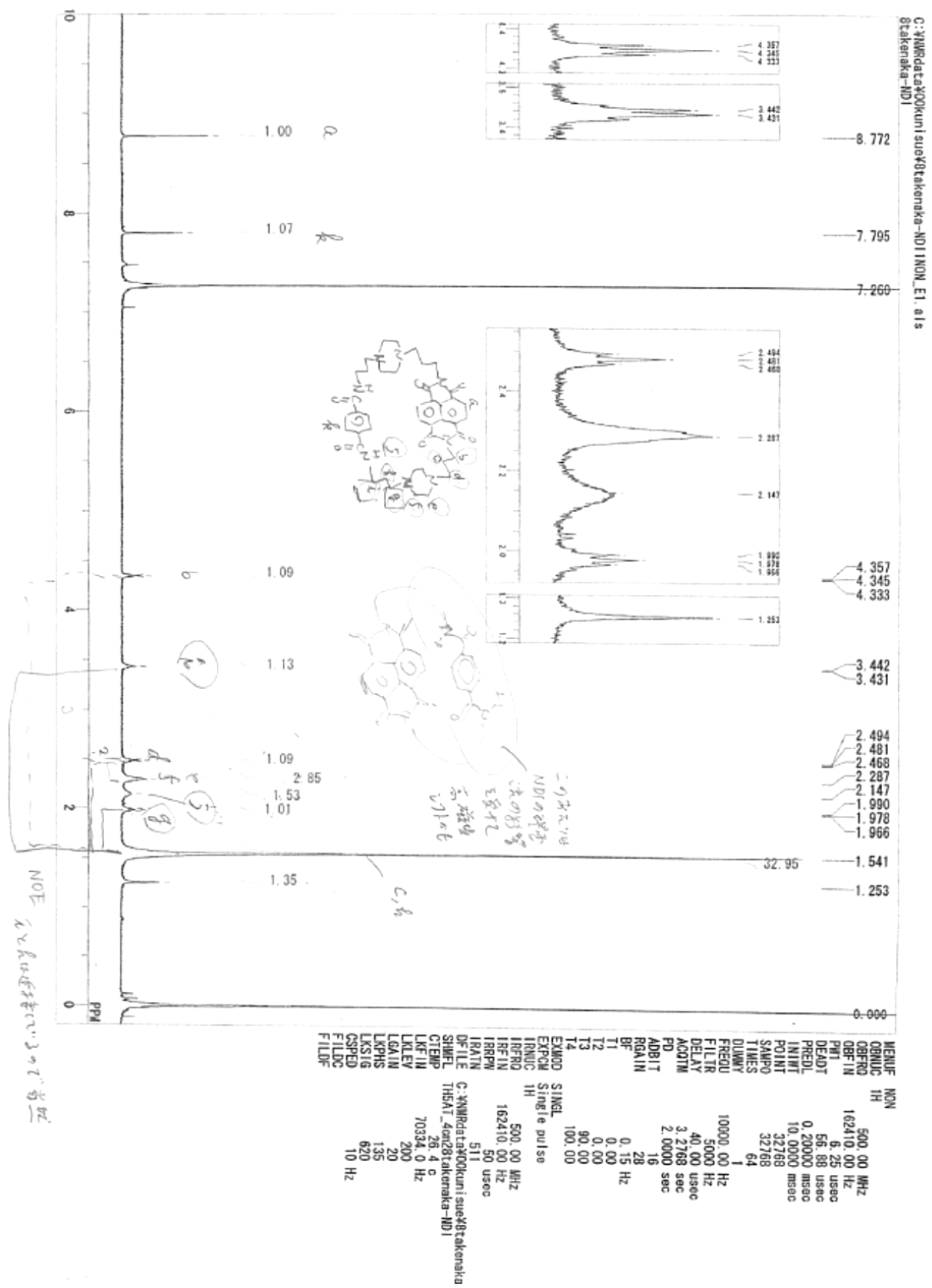


**Figure S2.**  $^1\text{H}$ -NMR chart of cNDI **1** in  $\text{CDCl}_3$  using TMS as internal standard.

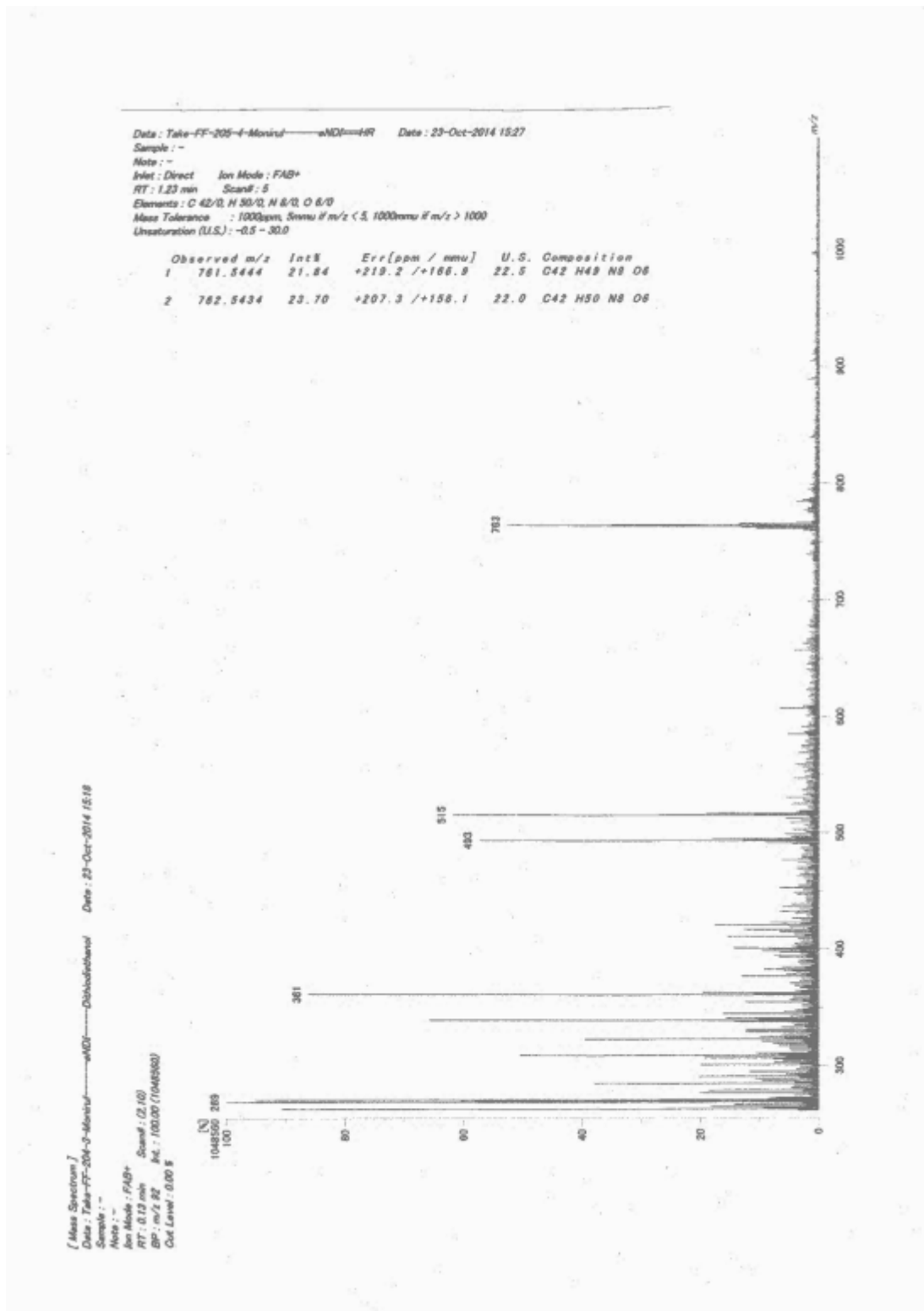


**Figure S3.** High-resolution mass spectra (HRMS-FAB) of cNDI 1.

### Synthesis of cNDI **2**

A solution of **5** 1.1 g (0.9 mmol), terephthalic acid 0.15 g (0.9 mmol), triethylamine 15 mL, 1-hydroxybenzotriazole (HOBT) 0.12 g (0.9 mmol), 1-Ethyl-3-(3-dimethylaminopropyl)-carbodiimide hydrochloride 0.17 g (0.09 mmol) in  $\text{CHCl}_3$  400 mL was stirred at room temperature and the progress of this reaction was monitored by TLC on silica gel with mixture of  $\text{CHCl}_3$ : diethylamine : Methanol = 10 : 0.2 : 1.0 as developing agent. After 48 h stirring, the reaction mixture was evaporated under reduced pressure and the residue was dissolved with 100 mL  $\text{CHCl}_3$ . After filtration and subsequently washed with sat.  $\text{NaHCO}_3$  aq. (80 ml $\times$ 5), and dried over magnesium sulfate. The solvent was removed and the residue was chromatographed on a silica gel column (Merck60) using the eluent of  $\text{CHCl}_3$ : diethylamine : Methanol = 10 : 0.2 : 1.0. The fraction of  $R_f = 0.41$  was collected and the solvent was removed under reduced pressure. The obtained residue was recrystallized from ethyl acetate, and cNDI **2** was obtained as brown crystal with 17 mg (yield, 3%). MALDI-TOFMS (positive mode,  $\alpha$ -CHCA)  $m/z = 653.54$  (theory for  $\text{C}_{36}\text{H}_{40}\text{N}_6\text{O}_6 + \text{H}^+ = 653.302$ ).  $^1\text{H}$  NMR (500 MHz,  $\text{CDCl}_3$ , TMS)  $\delta$  1.34 (4H, m), 1.5 (4H, t,  $J=5.9$ ), 1.87 (4H, m), 2.09 (6H, s), 2.31 (4H, m) 3.16 (4H, m), 4.12 (4H, t,  $J=6.8$ ), 7.12 (2H, s), 7.56 (4H, s), 8.71 (4H, s) ppm. HRMS Calcd. for  $\text{C}_{36}\text{H}_{40}\text{N}_6\text{O}_6 + \text{H}^+$ : M, 653.302. Found:  $m/z$  653.302. 1 mM cNDI **2** aqueous solution was prepared as estimation from the molar absorptivity of 28800  $\text{cm}^{-1}\text{M}^{-1}$  at 384 nm.

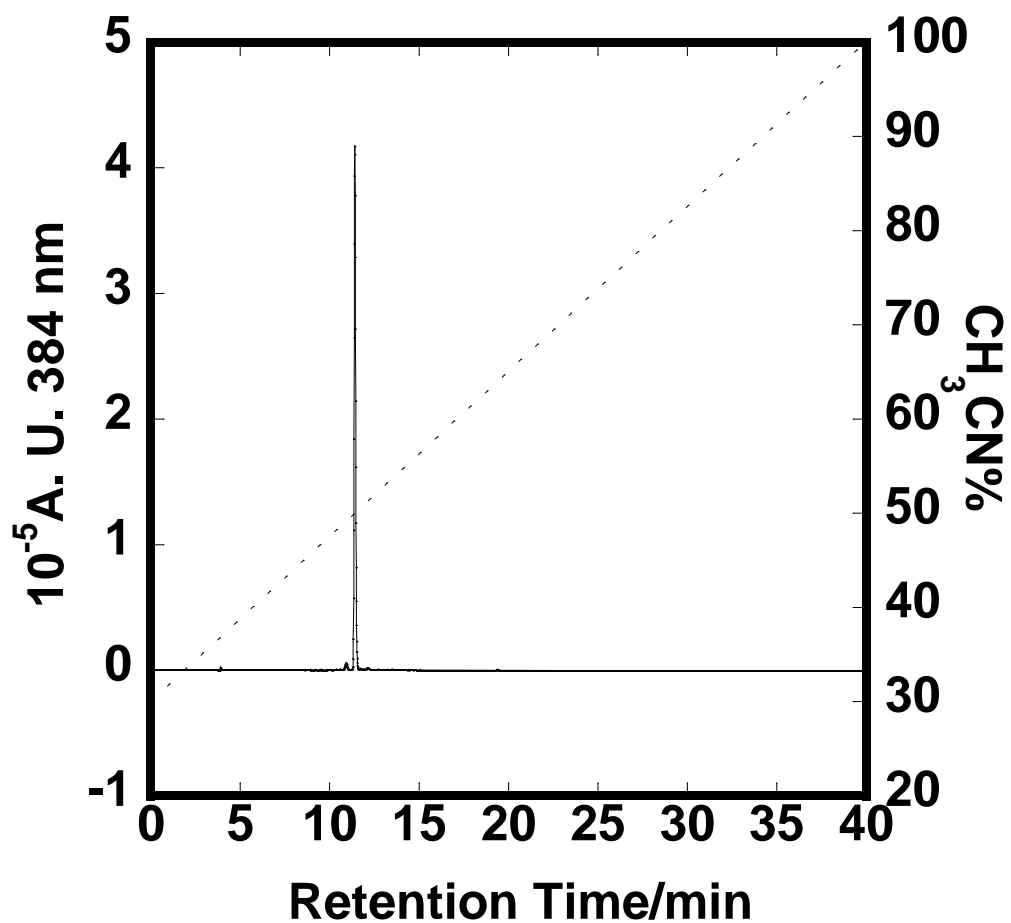


**Figure S4.** Reversed phase HPLC of cNDI 2. The concentration of acetonitrile was changed linearly to 100% from 29% in water containing 0.1% trifluoroacetic acid over 40 min at 40 °C

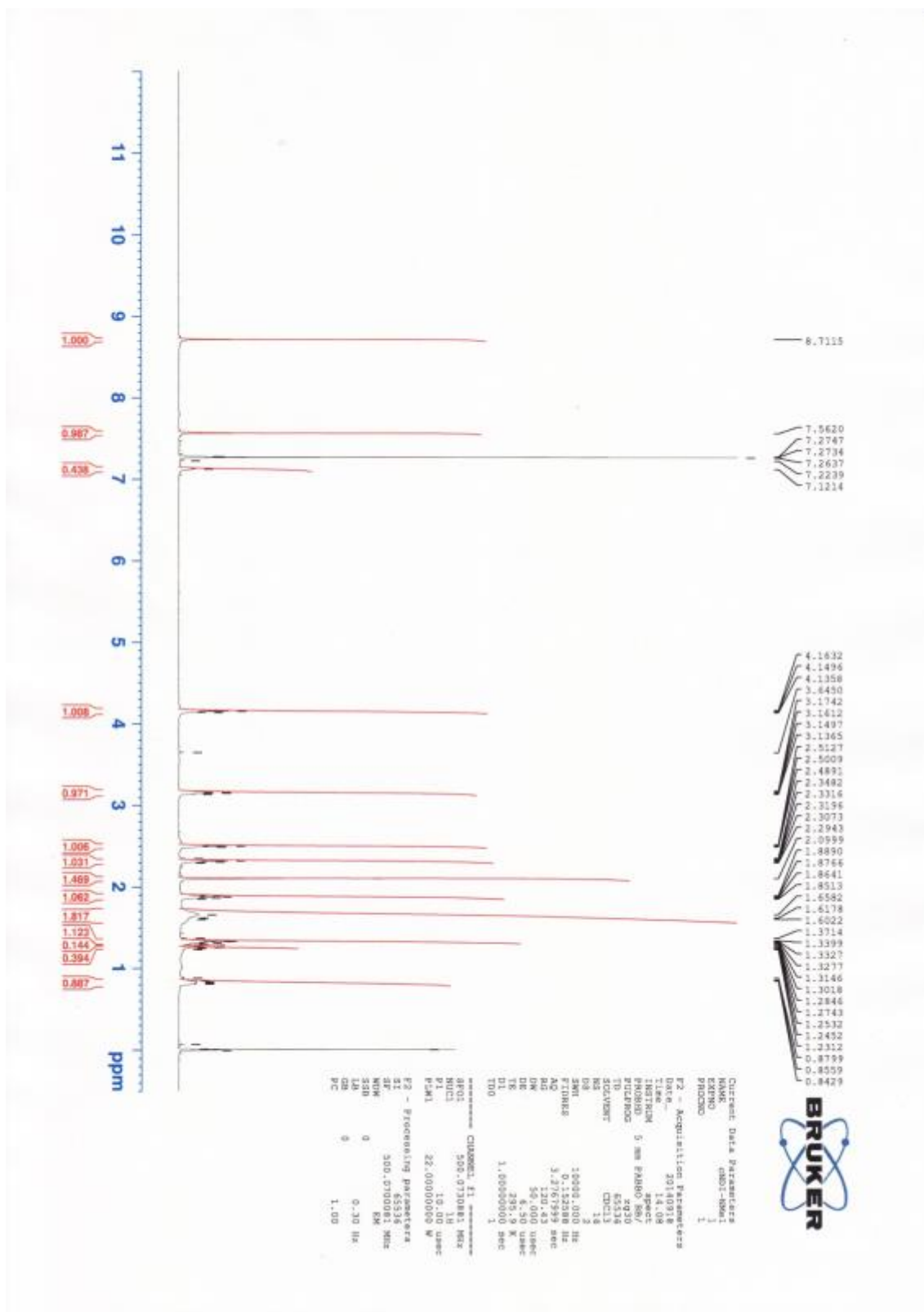
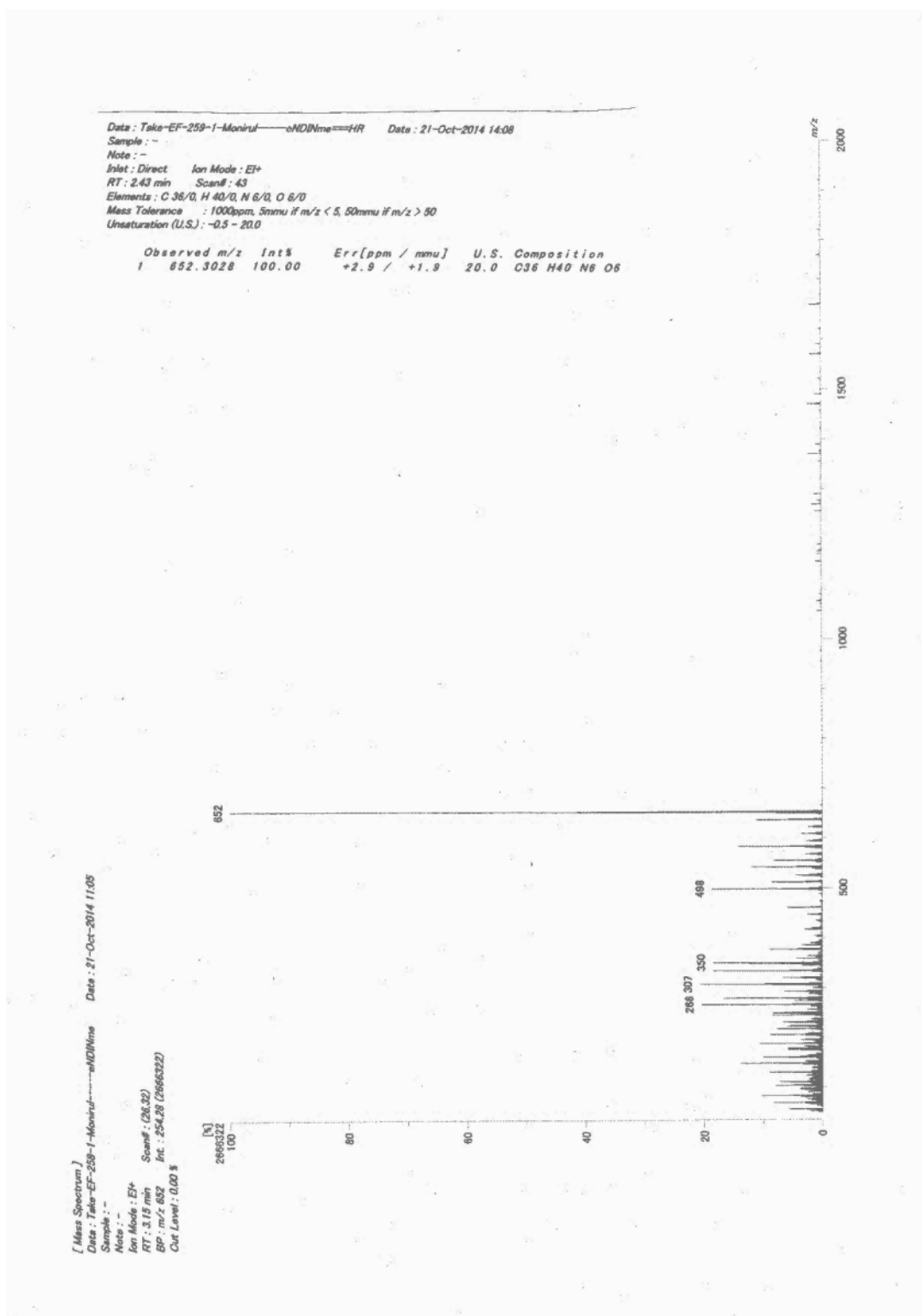
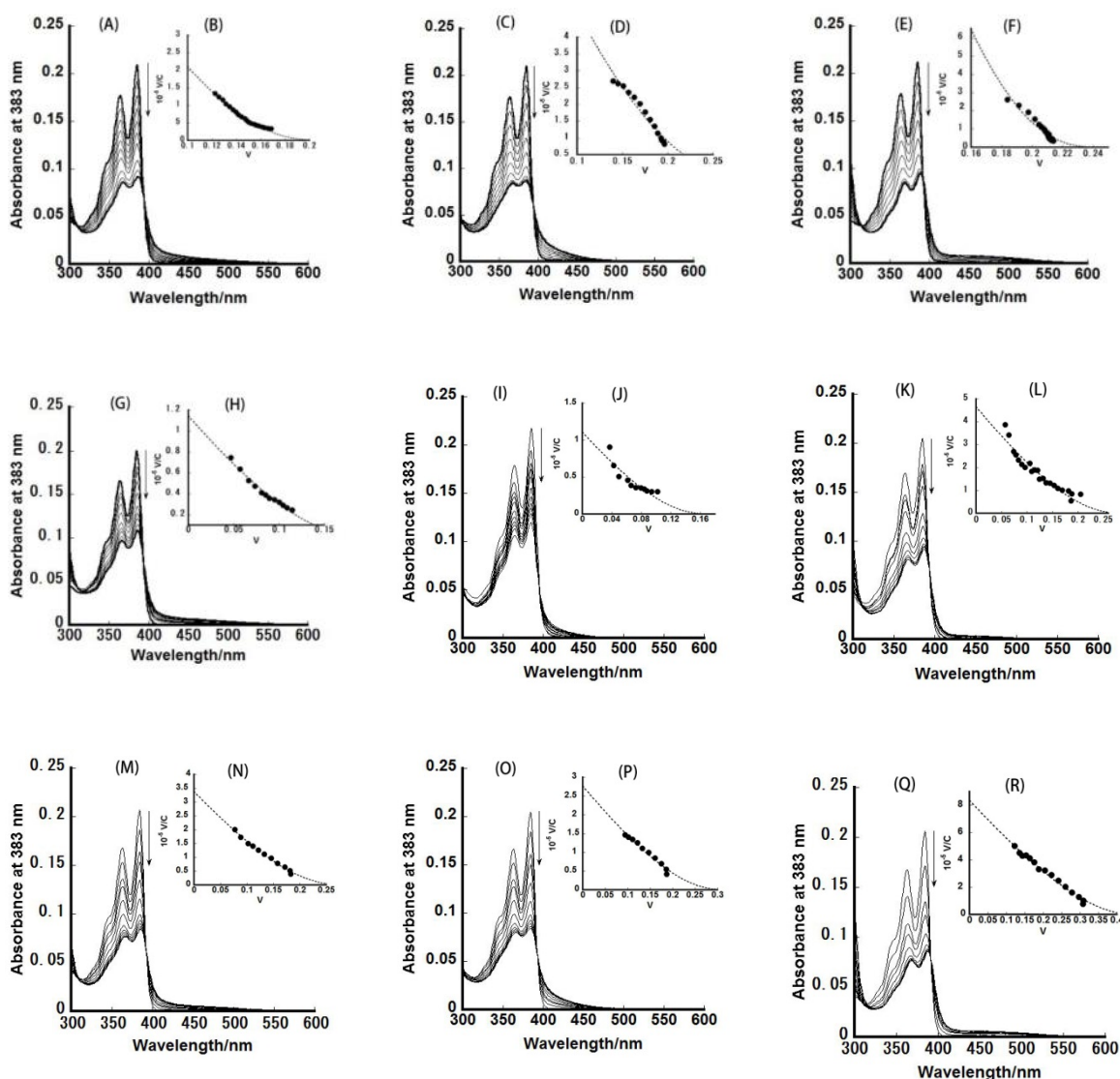


Figure S5. <sup>1</sup>H-NMR chart of cNDI 2 in CDCl<sub>3</sub> using TMS as internal standard.



**Figure S6.** High-resolution mass spectra (HRMS-EI<sup>+</sup>) of cNDI 2.



**Fig. S7.** UV-Vis absorption spectra of 6.7  $\mu\text{M}$  cNDI 1 (A, C, E), cNDI 2 (G, I, K) or non-cyclic NDI 3 (M, O, Q) in the absence and presence of titrant calf thymus DNA (A, G, M), Poly (dA-dT)<sub>2</sub> (C, I, O) and Poly (dG-dC)<sub>2</sub> (E, K, Q) with 0, 5, 10, 15, 20, 25, 30, 40 and 50  $\mu\text{M}$  respectively. Binding affinities were estimated using the scatchard plot of cNDI 1 (B, D, F), cNDI 2 (H, J, L) or non-cyclic NDI 3 (N, P, R) using the titrant calf thymus DNA (B, H, N), Poly (dA-dT)<sub>2</sub> (D, J, P) and Poly (dG-dC)<sub>2</sub> (F, L, R). Experiments were performed at 25°C in 10 mM MES buffer pH 6.25 containing 100 mM NaCl and 1 mM EDTA.

**Table S1**

Summary of the optical properties of free and DNA bound cNDI derivatives **1-3**.

DNAs	CT-DNA			Poly [d(A-T)] <sub>2</sub>			Poly [d(G-C)] <sub>2</sub>		
	<b>1</b>	<b>2</b>	<b>3</b>	<b>1</b>	<b>2</b>	<b>3</b>	<b>1</b>	<b>2</b>	<b>3</b>
ligands									
$\lambda_{max}$ (free)	383	383	383	383	383	383	383	383	383
$\lambda_{max}$ (bound)	387	386	388	387	386	387	388	385	388
$\lambda_{iso}$	395	395	393	394	396	392	392	393	391
H%	60	60.4	61.7	47.43	49.2	59.5	61.3	61	61.3

Units:  $\lambda$  nm.

$\lambda_{iso}$ : Wavelength at the isosbestic point

H: Hypochromicity, measured by using the formula

$$H\% = \frac{\text{Absorbance at 383nm (free)} - \text{Absorbance at 383nm (bound)}}{\text{Absorbance at 383nm (free)}} \times 100^1$$

1. N. Shahabadi, A. Fatahi, Multispectroscopic DNA-binding studies of a tris-chelate nickel(II) complex containing 4,7-diphenyl 1,10-phenanthroline ligands, J. Mol. Struct. 970 (2010) 90–95.

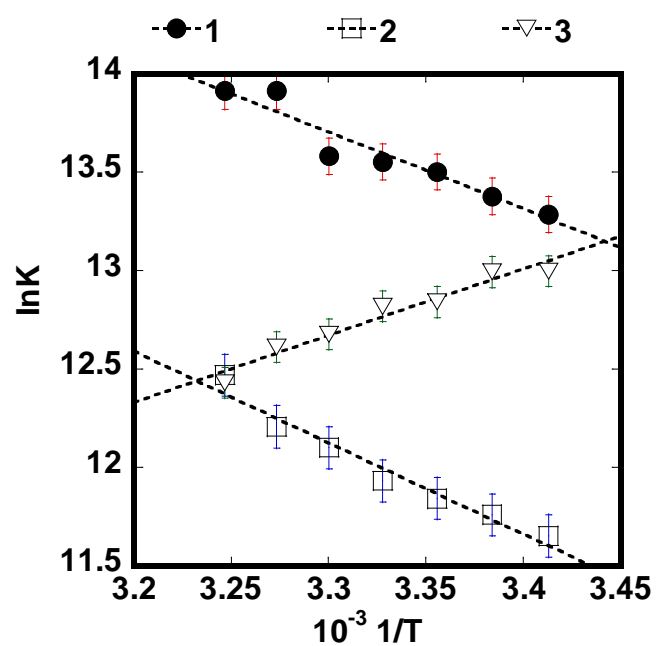


**Fig. S8.** Plots of  $\ln K$  (the observed equilibrium constants) vs  $1/T$  under the binding of cNDI derivatives **1-3** to calf thymus DNA.

**Table S2**

Binding constants of cNDI derivatives **1-3** interacting with calf thymus DNA at different temperature.

Temperature (°C)	$10^{-5}K_b/M^{-1}$		
	<b>1</b>	<b>2</b>	<b>3</b>
20	5.9 ( $\pm 0.24$ )	1.15 ( $\pm 0.4$ )	4.5 ( $\pm 0.12$ )
22.5	6.5 ( $\pm 0.25$ )	1.28 ( $\pm 0.4$ )	4.4 ( $\pm 0.12$ )
25	7.0 ( $\pm 0.23$ )	1.40 ( $\pm 0.7$ )	3.8 ( $\pm 0.11$ )
27.5	7.7 ( $\pm 0.23$ )	1.52 ( $\pm 0.12$ )	3.7 ( $\pm 0.07$ )
30	7.9( $\pm 0.5$ )	1.8( $\pm 0.05$ )	3.2( $\pm 0.2$ )
32.5	11( $\pm 1$ )	2( $\pm 0.18$ )	3( $\pm 0.15$ )
35	11( $\pm 1.5$ )	2.6( $\pm 0.1$ )	2.5( $\pm 0.2$ )

Condition: 10 mM MES (pH6.25), 1 mM EDTA, and 0.1 M NaCl.

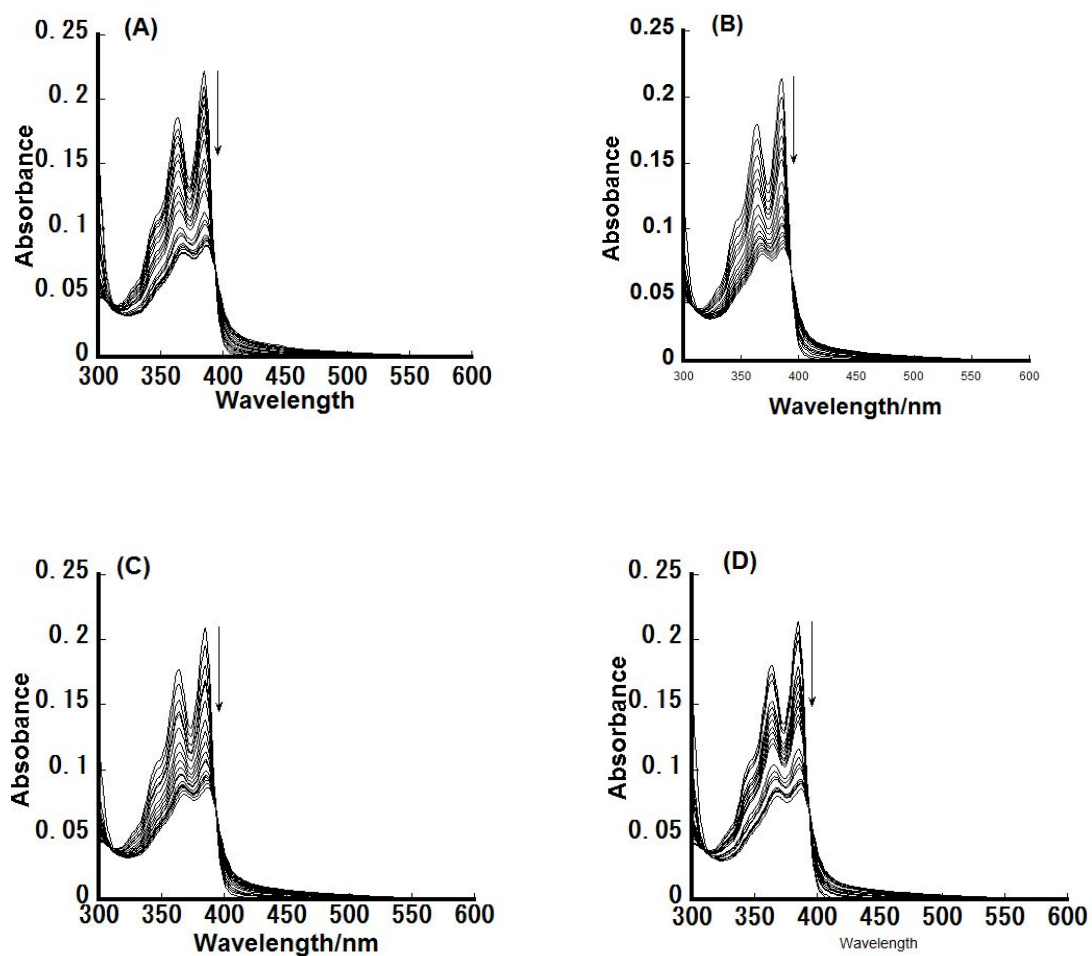


**Fig. S9.** UV-Vis absorption spectra of 6.7 μM cNDI 1 in the absence and presence of titrant calf thymus DNA. Experiments were performed at 20°C (A), 22.5°C (B), 25°C (C), 27.5°C (D) in 10 mM MES buffer pH 6.25 containing 100 mM NaCl and 1 mM EDTA.

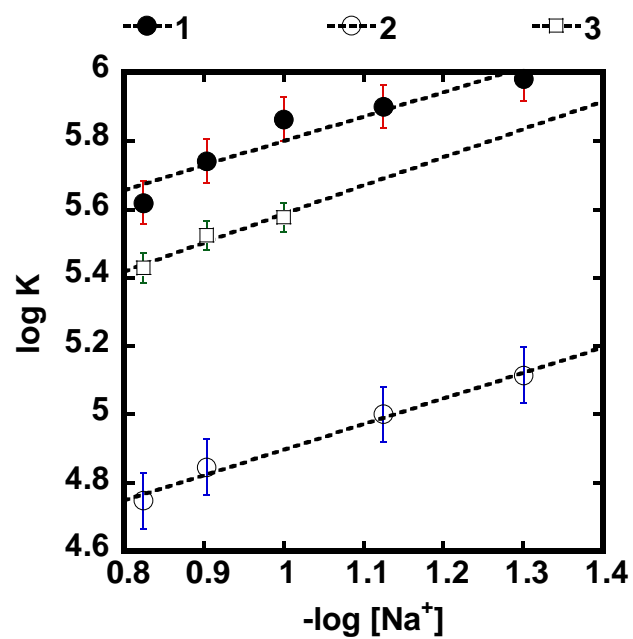


**Fig. S10.** Plots of  $\log K$  (the observed equilibrium constants), versus  $-\log[\text{Na}^+]$  under the binding of cNDI derivatives **1-3** to calf thymus DNA.

**Table S3**

Binding constants of cNDI derivatives **1-3** interacting with calf thymus DNA at different salt concentration.

[NaCl]/M	$10^{-5}K_b/M^{-1}$		
	<b>1</b>	<b>2</b>	<b>3</b>
0.05	9.56	1.3	-
0.075	7.94	1.0	-
0.1	7.29	1.3	1.30
0.125	5.50	0.7	0.95
0.15	4.15	0.56	0.56

Condition: 10 mM MES (pH6.25), 1 mM EDTA, and 0.05-0.15 M NaCl.

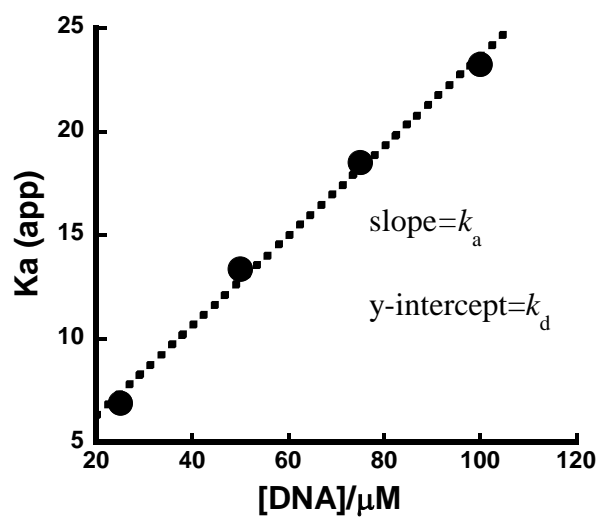
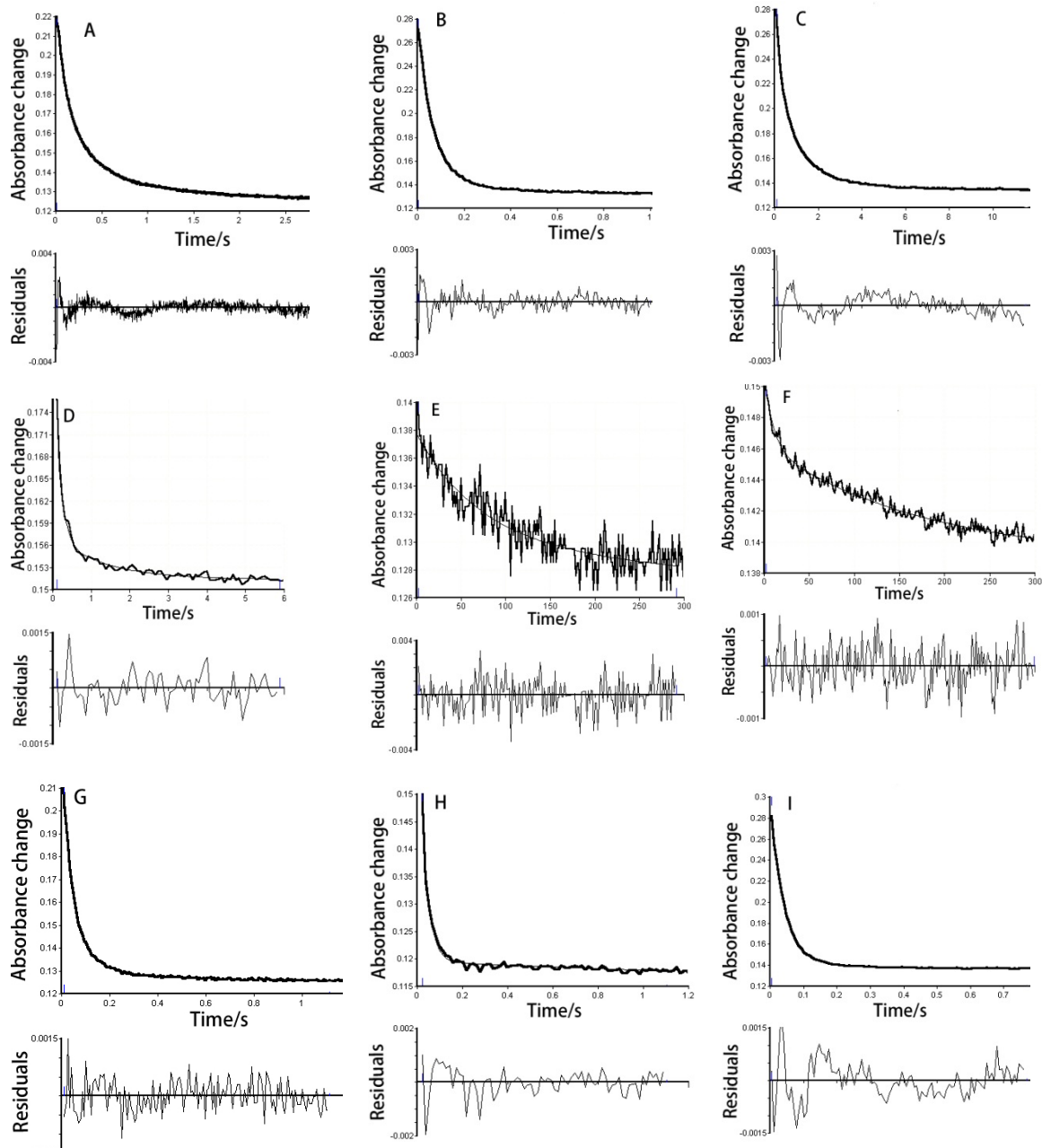
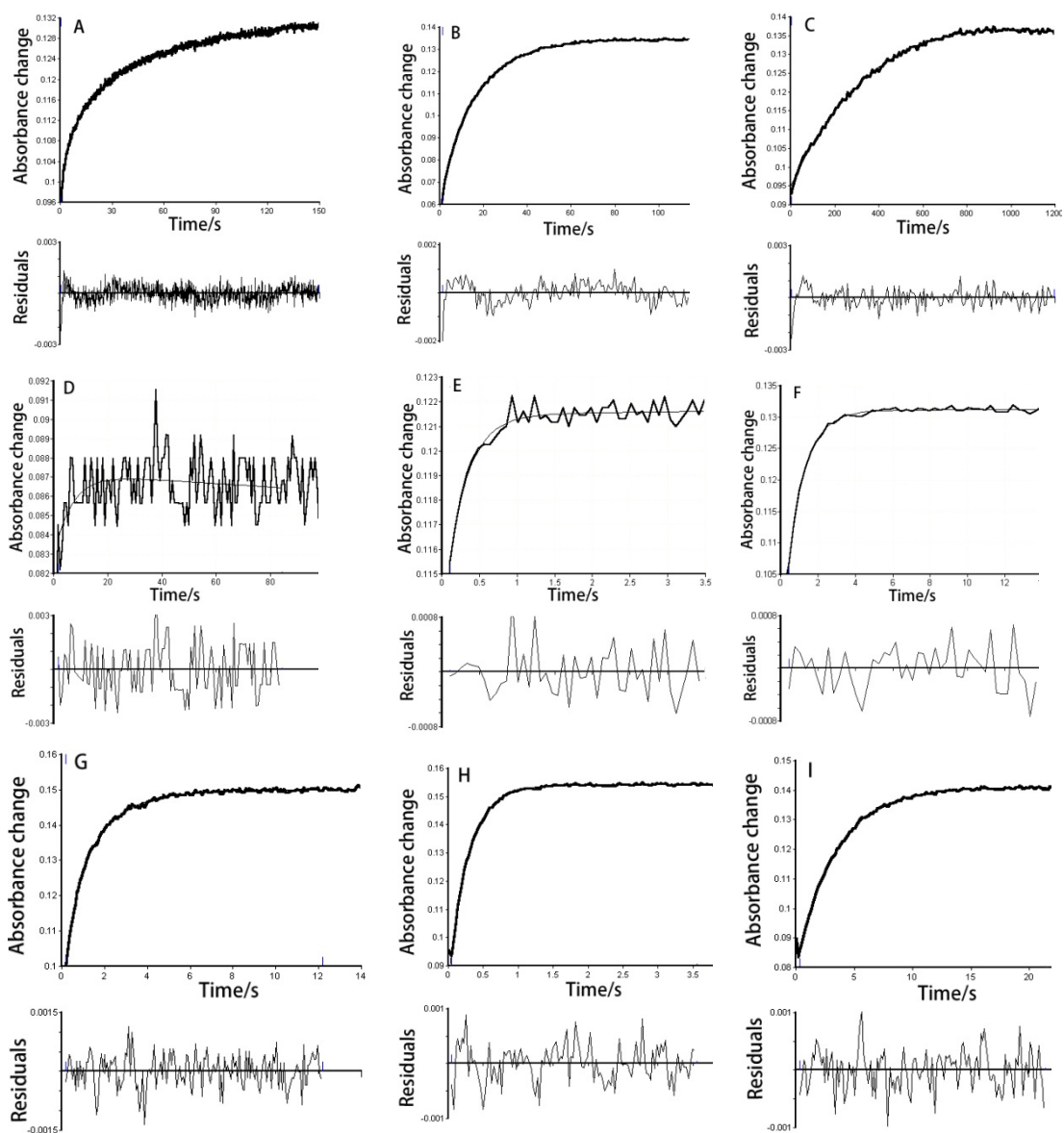


Fig. S11. Plot of the apparent rate constants ( $K_{app}$ ) against DNA concentrations, with the  $K_{app}$  determined by fitting the absorbance changes at 383 nm to a single-exponential decay.



**Figure S12.** Stopped-flow kinetics traces for association of cNDI 1 (A, B, C), cNDI 2 (D, E, F) and non-cyclic NDI 3 (G,H,I) from calf thymus DNA (A, D, G), from Poly [d(A-T)]<sub>2</sub> (B, E, H) and from Poly [d(G-C)]<sub>2</sub> (C, F, I). The experiments were conducted in 10 mM MES buffer and 1 mM EDTA (pH 6.25) containing 100 mM NaCl. [Ligand]/[DNA/bp] =1:10



**Figure S13.** Stopped-flow kinetics traces for SDS driven dissociation of cNDI 1 (A, B, C), cNDI 2 (D, E, F) and non-cyclic NDI 3 (G, H, I) from calf thymus DNA (A, D, G), from Poly [d(A-T)]<sub>2</sub> (B, E, H) and from Poly [d(G-C)]<sub>2</sub> (C, F, I). The experiments were conducted in 10 mM MES buffer pH 6.25 containing 100 mM NaCl and 1 mM EDTA. [Ligand]/ [DNA/bp] =1:10

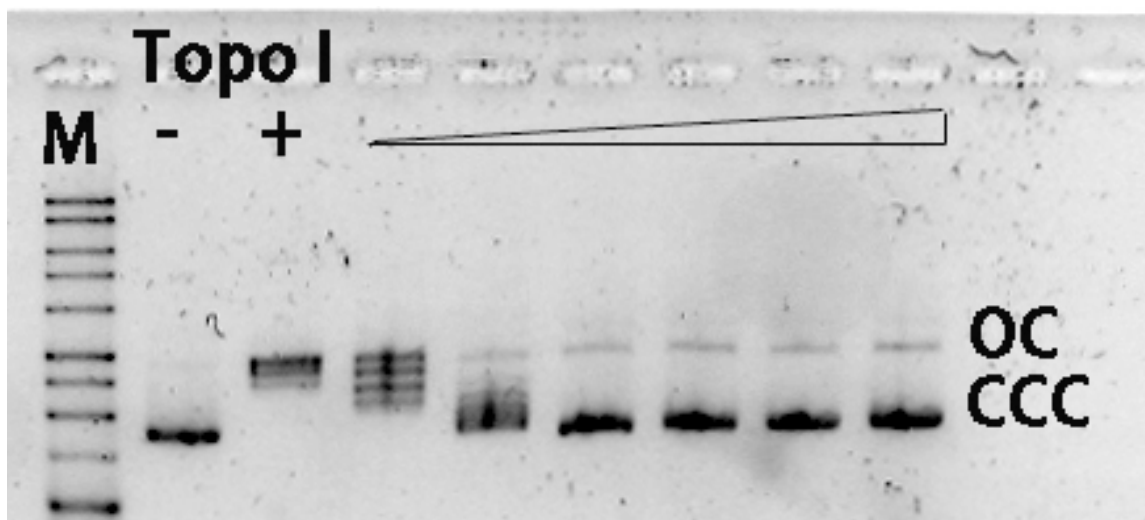


**Fig. S14.** Topoisomerase I assay for pUC19 treated with 5.0 U of enzyme. Following incubation at various concentrations of cNDI 2 (2.0, 5.0, 10, 20, 30, 40, 50  $\mu$ M from left to right) was added and the mixture incubated further. After work-up, DNA was electrophoresed. Lanes M and Topo I represent 1 kb size markers and pUC19 respectively. OC and CCC refer to open circle and the covalent closed circle respectively.